

Power-Law-Exponential Interaction Induced Quantum Spiral Phases

Guoqing Tian,¹ Ying Wu,¹ and Xin-You Lü^{1,*}

¹*School of Physics and Institute for Quantum Science and Engineering,
Huazhong University of Science and Technology and Wuhan Institute of Quantum Technology, Wuhan 430074, China*
(Dated: May 24, 2024)

We theoretically predict a kind of power-law-exponential (PLE) dipole-dipole interaction between quantum emitters in a 1D waveguide QED system. This unconventional long-range interaction is the combination of power-law growth and exponential decay couplings. Applying PLE interaction to a spin model, we uncover the rich many-body phases. Most remarkably, we find that PLE interaction can induce the ordered and critical spiral phases. These spiral phases emerge from the strong frustration generated by the power-law factor of PLE interaction, hence they are absent for other types of long-range interaction, e.g., pure exponential and power-law decay interactions. Our work is also applicable for the higher dimensional systems. It fundamentally broadens the realm of many-body physics and has the significant applications in quantum simulation of strong correlated matters.

The studies on many-body behaviors of quantum matters are fundamentally important both in theoretical and experimental respects. In the framework of Ginzburg-Landau theory, the many-body interactions play a key role to induce intriguing phenomena, i.e., quantum phases and phase transitions [1–3]. Significant progress has been made in understanding many-body phases in systems with short-range interactions, while long-range interacting systems have continuously attracted research attention as they can induce distinctive phases without counterparts in short-range interacting systems [4–9]. For example, long-range interactions can give rise to Wigner crystallization [10], and continuous symmetry broken in low-dimensional systems [11–13].

Waveguide QED system where QEs couple to a structured bosonic environment, provide a platform to efficiently generate long-range interactions [14–17]. In particular, mediated by a 1D bipartite photonic lattice, the spatial profile of emergent long-range dipole-dipole (d-d) interactions between QEs exhibits the topological edge state features as the frequency of QEs is resonant with the edge state energy of lattice [5, 10, 18, 21]. Especially, the non-monotonic d-d interaction emerges in the extended SSH lattice [11]. This provides an opportunity to explore exotic phases of matter induced by these long-range interactions [23].

In this work, we investigate the system consists of QEs coupling to a 1D bipartite photonic lattice endowed with chiral symmetry. By integrating hopping terms beyond nearest-neighbor into lattice and appropriately designing the hopping strengths, we predict a kind of power-law-exponential d-d interactions featuring with non-monotonicity. Different from the previous work [11] reporting the d-d interaction featuring non-monotonic spatial behavior, here the non-monotonicity of PLE interactions entirely comes from the power-law increasing term x^α . Mathematically, such power-law factor originates from the existence of higher order zeros in the characteristic polynomial of bath. Physically, it is the

consequence of the interference between multiple exponential decay components of interaction with the same decay length.

More importantly, applying the long-range PLE interaction to an effective spin model, we uncover the rich many-body phases in this system for the first time. Especially, as the interaction length increasing, we find a quantum critical phase, i.e., the quasi-long-range ordered phase (QLRO(T)) with T indicating the wave number of the dominant spin correlations. Distinctive from the other critical phase occurring for short interaction length, the spin-spin correlation function in QLRO(T) phase is spiral with distance, and has the incommensurate period T. In addition, an ordered spiral phase named antiferromagnetic phase with period T (AFM(T)) also appears when the spin-exchange interaction is ignorable in comparison with zz interaction. Similar to the QLRO(T) phase, the spin arranges antiferromagnetically in this AFM(T) phase but with commensurate periods. We explain that these spiral phases emerge from the strong frustration induced by the power-law increasing factor of interaction, and thus has no analog in other kinds of long-range interaction (e.g., exponential and power-law decay interactions) systems. Our work open up a door for exploring unconventional long range interactions by employing the topological property of bath, which is fundamentally significant in realizing the novel many-body phases.

PLE d-d interaction mediated by chirally symmetric lattice.—As shown in Fig. S1(a), we consider N two-level QEs coupled to 1D photonic two-sublattice bath. The total Hamiltonian of system reads (setting $a_0 = 1$)

$$H_N = \omega_q \sum_{j=1}^N \sigma_j^\dagger \sigma_j + H_b + \lambda \sum_{j=1}^N (a_{x_j, \alpha}^\dagger \sigma_j + h.c.), \quad (1)$$

where ω_q is the transition frequency of QEs, and λ is the coupling strength. Moreover, $\sigma_j = |g\rangle_j \langle e|$ is the Pauli annihilation operator for the j -th emitter, and $a_{x_j, \alpha}$ is the

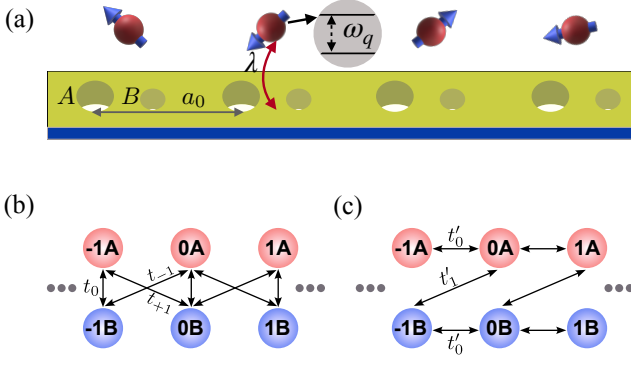


FIG. 1: (a) N two-level QEs coupled to 1D coupled-cavity array, where two adjacent cells are separated by a_0 . (b) Real space configuration of the lattice bath for $h(k) = t_0 + t_{-1} \exp(-ik) + t_{+1} \exp(ik)$ with the hopping strengths $\{t_0; t_{-1}; t_{+1}\}$ and thus $P = 1$, $Q = 1$. (c) Real space configuration of the lattice bath for $H(k) = t'_1 \sin(k) \sigma_y + (t'_0 \cos(k) + m_0) \sigma_z$, which respects the chiral symmetry σ_x and is able to produce the d-d interaction without chirality.

annihilation operator corresponding to the position $x_{j,\alpha}$ of bath (i.e., sublattice $\alpha \in \{A, B\}$ at the x_j -th cell). Under periodic boundary condition, the bath Hamiltonian is given by $H_b = \sum_k \begin{pmatrix} a_{k,A}^\dagger & a_{k,B}^\dagger \end{pmatrix} H_b(k) \begin{pmatrix} a_{k,A} \\ a_{k,B} \end{pmatrix}^T$ with $H_b(k) = \omega_0 \mathbb{I} + d_x(k) \sigma_x + d_y(k) \sigma_y + d_z(k) \sigma_z$. We consider the bath respecting a chiral symmetry $\sigma_z(H_b(k) - \omega_0 \mathbb{I}) \sigma_z = -(H_b(k) - \omega_0 \mathbb{I})$ (hence $d_z(k) = 0$). The full property of the lattice bath is encoded in $h(k) = d_x(k) - i d_y(k)$, whose generic form can be written as $h(k) = \sum_{m=0}^P t_{-m} e^{-imk} + \sum_{n=0}^Q t_{+n} e^{ink}$ with the hopping strengths of lattice $\{t_0; t_{-1}, \dots, t_{-P}; t_{+1}, \dots, t_{+Q}\}$. The integer P (Q) denotes the at most P -site (Q -site) hopping from sublattice A to B towards the left (right) direction [see Fig. S1(b) for an example].

In the single-excitation regime, when a single QE with frequency $\omega_q = \omega_0$ couples to bath at $x_{1,\alpha}$, a vacancy-like bound state with eigenenergy $E = \omega_0$ occurs [5]. When the second QE located at $x_{2,\beta}$ is integrated into the bath, the mechanism of vacancy-like bound state guarantees the resulted d-d interaction has the same spatial profile with the zero-energy state of H_b (we set $\omega_q = \omega_0 = 0$ for simplify), i.e., $J(x_{1,\alpha}, x_{2,\beta}) \propto \lambda \langle x_{2,\beta} | \varphi_E \rangle$, where $|\varphi_E\rangle$ is the zero-energy solution of bath under hard-core boundary condition [24]. Without loss of generality, we assume that the first QE couples to bath at sublattice A of the 0-th cell. We ignore the case of which the second QE couples to bath at sublattice A, since the obtained d-d interaction is zero due to the chiral symmetry σ_z , and we use the short notation $J(x) = J(x_{2,B} - x_{1,A}) \equiv J(x_{1,A}, x_{2,B})$. In thermodynamic limit of bath, we obtain a unified form of d-d interaction by solving the zero-energy state. The

expression is given by [25]

$$\frac{J(x)}{\lambda} \propto \begin{cases} \sum_{\mu=1}^{n_\mu-1} \sum_{\alpha=0}^{n_\mu-1} r_{\mu\alpha} (x - x_c)^\alpha e^{-(x-x_c)/\xi_\mu}, & x \geq x_c, \\ \sum_{\nu=1}^{n_\nu-1} \sum_{\beta=0}^{n_\nu-1} l_{\nu\beta} (x - x_c)^\beta e^{-(x-x_c)/\xi_\nu}, & x < x_c, \end{cases} \quad (2)$$

where $x_c = 1 - P$, $r_{\mu\alpha}$ and $l_{\nu\beta}$ are constants, and the summation indexes μ, ν cover all distinctive zeros $z_{\mu,\nu}$ of the characteristic polynomial $h(z)$ obtained from $h(k \rightarrow -i \ln z)$ in complex plane. Here $n_{\mu,\nu}$ is the order of $z_{\mu,\nu}$, and $\xi_{\mu,\nu} = -\ln^{-1}(z_{\mu,\nu})$ is the decay length of interaction. All physical quantities mentioned here are exactly solvable and are determined by the bulk property of bath.

Since the power-law factor $(x - x_c)^{\alpha,\beta}$ in Eq. (2), the strength of PLE interaction is weakened at short range and enhanced at long range comparing with the pure exponential decay interaction. Its maximal strength locates at $x = \alpha \xi_\mu - x_c$. The occurrence of power-law factor originates mathematically from the higher-order zero of $h(z)$. Since the maximal order of zero should be less than or equal to the number of zeros, we obtain the upper bounds on the power-law exponents

$$\max_{\text{Re } \xi_\mu > 0} \{n_\mu\} \leq P + W, \quad \max_{\text{Re } \xi_\nu < 0} \{n_\nu\} \leq Q - W, \quad (3)$$

where $W = (2\pi i)^{-1} \int_0^{2\pi} \partial_k \log(h(k)) dk$ is the winding number characterizing the topology of bath. Physically, the value of $P + W$ ($Q - W$) counts the number of zeros of $h(z)$ lying within (outside) the unit circle, and then it is equal to the number of exponential decay components involved in the superposition of d-d interaction. When the lattice is further engineered such that n_μ (n_ν) out of $P + W$ ($Q - W$) exponential decay components of interaction possess the same decay length, the interference between n_μ (n_ν) exponential decay components leads to the PLE interaction towards to $x > x_c$ ($x < x_c$) direction with maximal exponent $n_\mu - 1$ ($n_\nu - 1$). The detailed calculation and discussion are shown in Supplemental Material [25].

Minimal model exhibiting PLE interaction.—We present an example to demonstrate the physical mechanism of realizing PLE interaction more clearly. To this end, considering an extended SSH bath with $h(k) = t_0 + t_{-1} \exp(-ik) + t_{+1} \exp(ik)$. In addition to the nearest neighbor hopping t_0 and t_{-1} , we introduce the next-next (NN) nearest hopping t_{+1} into bath. For hopping strengths $t_0^2 \neq 4t_{+1}t_{-1}$, the d-d interaction mediated by this bath yields [25]

$$\frac{J(x)}{\lambda} \propto \begin{cases} \frac{r(\xi_1) e^{-x/\xi_1} - r(\xi_2) e^{-x/\xi_2}}{e^{-1/\xi_1} - e^{-1/\xi_2}}, & x \geq 0 \\ \frac{l(\xi_1) e^{-x/\xi_1} - l(\xi_2) e^{-x/\xi_2}}{e^{-1/\xi_1} - e^{-1/\xi_2}}, & x < 0 \end{cases} \quad (4)$$

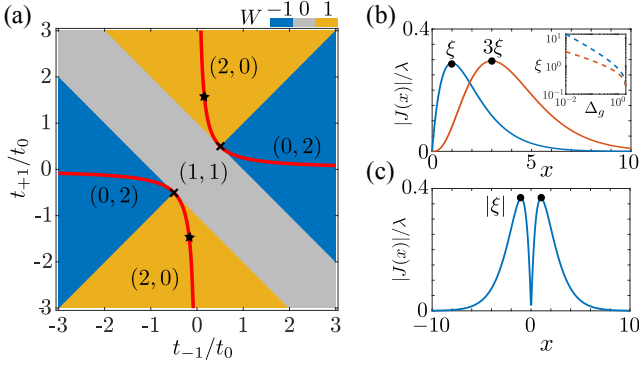


FIG. 2: (a) Phase diagram of the lattice bath. Red line $4t_{+1}t_{-1} = t_0^2$ is the parameter regime for PLE interaction. The cross marks label two tri-phase points, where the PLE interaction is absent. The integer pairs are the upper bounds $(P + W, Q - W)$. (b) Spatial profile of PLE interaction $x \exp(-x/\xi)$ (blue line) with right-hand chirality that corresponds to the parameters denoted by black stars in (a). The orange line displays PLE interaction $x^3 \exp(-x/\xi)$, the lattice configuration is given in [25]. Inset displays the decay length ξ versus the band gap of lattice bath Δ_g/t_0 for power-law factor 1 (dashed blue line) and 3 (dashed orange line). (c) PLE interaction without chirality $|x| \exp(-|x|/\xi)$ with lattice configuration giving in Fig. S1(c). In (b-c), the dots mark the positions of maximum interaction strength.

where $r(z) = \Theta(1 - |\exp(1/z)|) \text{sign}(1 - |\exp(1/z)|)$, $l(z) = \Theta(-1 + |\exp(1/z)|) \text{sign}(1 - |\exp(1/z)|)$, and $\xi_{1,2} = -1/\ln(z_{1,2})$. Here $z_1 = (-t_0 + (t_0^2 - 4t_{+1}t_{-1})^{1/2})/2t_{+1}$, $z_2 = (-t_0 - (t_0^2 - 4t_{+1}t_{-1})^{1/2})/2t_{+1}$ are the zeros of $h(z)$, and $\Theta(x)$ is the Heaviside function. It is shown from Eq. (4) that a zero lying within (outside) the unit circle contributes an exponential decay component. Thus the d-d interaction is the superposition of two exponential decay components, when two zeros lie simultaneously within or outside the unit circle. As the hopping strengths being engineered such that the condition for PLE interaction $4t_{+1}t_{-1} = t_0^2$ is satisfied, two zeros coincide and Eq. (4) becomes intermediate. Then, one needs to take the limit to obtain the interaction (suppose $\text{Re}(\xi_{1,2}) > 0$), i.e.,

$$\frac{J(x \geq 0)}{\lambda} \propto \lim_{\xi_{1,2} \rightarrow \xi} \frac{e^{-x/\xi_1} - e^{-x/\xi_2}}{e^{-1/\xi_1} - e^{-1/\xi_2}} \propto x e^{-x/\xi}. \quad (5)$$

This formula indicates the underlying interference mechanism for PLE interaction with power-law exponent 1, namely the out-of-phase superposition of two exponential decay components with the same decay length ξ .

The phase diagram in Fig. S2(a) illustrates the parameter regimes for PLE interaction. Owing to the additional NN nearest hopping, the lattice bath has three phases distinguished by winding number 0 (topologically trivial) and ± 1 (topologically non-trivial). As indicated by Eqs. (2-3), the upper bounds larger than 1 is the necessary condition for the implement of PLE interaction.

Therefore, the parameter regimes for PLE interaction only appear in the topological phases in which one of the upper bounds is large than 1. Within these regimes, the hopping strengths should be properly engineered and satisfy the red lines to obtain PLE interaction. Fig. S2(b) shows the spatial profile of PLE interactions with power-law factors 1 and 3. As an indicator of non-monotonicity, the decay length ξ is controlled by the band gap of lattice according to the functional relation $\xi = -1/\ln(1 - (\Delta_g/2)^{1/\nu})$, where $\nu = n_\mu + 1$ for lattice producing power-law factor n_μ [26]. Note that, PLE interaction without chirality can also be obtained by coupling QEs to lattice bath with chiral symmetry σ_x [see Fig. S2(c)] [25]. Besides, our result in Supplemental Material [25] show the robustness of PLE interactions against symmetry-preserving disorder, and the realization of similar PLE interaction in higher dimensional lattice.

Based on this explicit model, the necessity of long-range hopping beyond nearest neighbor for the realization of PLE interaction becomes clear. Integrating longer-range hopping (increasing P and Q) into lattice will increase the values of upper bounds when keeping W invariant, and thus increase the number of components involving superposition. In other words, one needs to integrate longer range hopping into the lattice to produce potential PLE interaction with higher power-law exponents [25]. While for a SSH lattice (i.e., $t_{+1} = 0$), the upper bounds are at most equals to 1, which eventually leads to a pure exponential decay d-d interaction [18].

Spin many-body phases induced by PLE interaction.— The unique feature of PLE interaction in comparison with other types of long-range interaction, namely the power-law growth factor, inspires us to explore the emergent many-body phases. We consider a 1D long-range XXZ model described by the Hamiltonian $H_{XXZ} = \sum_{m>n}^N (m-n) \exp(-(m-n)/\xi) (S_m^+ S_n^-/2 + S_n^+ S_m^-/2 + J_z S_m^z S_n^z)$. The required zz interaction can be realized by the fast single-qubit rotations [27, 28].

In order to explore the many-body phases, we numerically calculate the entanglement entropy and spin-spin correlation [25] of the ground-state by using the DMRG method [29], and present the phase diagram in Fig. S3. When ξ is small (i.e short-range limit), the system reduces to nearest-neighbor interacting model. In this case, one finds a gapless XY phase known as the Tomonaga-Luttinger liquid for intermediate values of J_z [1, 2]. This critical phase, described by a conformal field theory with central charge $c = 1$ [9], exhibits algebraically decay correlation function. In the regime $J_z \gg 0$ ($J_z \ll 0$), one obtains an ordered antiferromagnetic (ferromagnetic) phase. When interaction length increases as the next-nearest-neighbor interaction becomes relevant, the system is effectively described by the J_1 - J_2 model [31]. A valence-bond-solid (VBS) phase emerges for intermediate values of J_z , which is identified by the exponentially

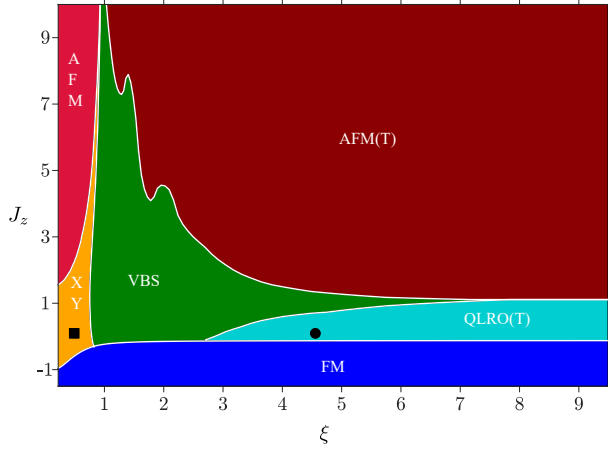


FIG. 3: (a) Phase diagram for the Hamiltonian $H_{XXZ} = \sum_{m>n} (m-n) \exp(-(m-n)/\xi) (S_m^+ S_n^- / 2 + S_n^+ S_m^- / 2 + J_z S_m^z S_n^z)$. The phase boundary from FM phase to other phases is obtained via a spin-wave analysis. Other phase boundaries are obtained by numerically calculate the effective central charge of ground state. More technical details about this phase diagram are given in [25]. The black square and circle markers denote the positions where spin correlation functions in Fig. S4(a) are drawn from.

decay spin correlation and long-range dimer correlation function [32]. We stress that all the above phases also exist in the exponential and power-law decay interacting systems [25]. The different forms of long-range interactions, however, modifies the boundaries between these phases.

We are more interested in the regime $\xi \gg 1$ where the power-law factor of PLE interaction becomes relevant. For intermediate value of J_z , system undergoes a phase transition from the VBS phase to a critical phase. This critical phase exhibits quite distinctive behavior from the XY phase appearing in short-range interacting limit. The spin correlation function $\langle S_i^+ S_j^- \rangle \sim |i-j|^{-\eta}$ decays with a rather slow power law (e.g., $\eta \approx 0.16$ at $\xi = 4.5$ and $J_z = 0$). Meanwhile, spin correlation is spiral with the incommensurate period T (T is not an integer) [see Fig. S4(a)]. Algebraic decay plus spiral behavior implies this critical phase is T-period quasi-long-range ordered phase (QLRO(T)). Besides, we find that the oscillation period T changes with interaction length. To characterize the relation between T and ξ , we further calculate the static structure factor in x - y plane $S_{xy}(q) = \langle S^+(q) S^-(q) \rangle$, where $S^-(q) = \sum_{m=1}^N \exp(-iqx_m) S_m^- / \sqrt{N}$ denotes a spin density wave operator with momentum $q \in \{0, 2\pi/N, 4\pi/N, \dots, (N-1)2\pi/N\}$. By numerically fitting the peaks of $S_{xy}(q)$, the approximate relation reads as $T(\xi) = 3/(1 - \exp(-1/\xi))$ for $J_z = 0$ [see Fig. S4(b)]. In addition, an antiferromagnetic ground state with the arrangement period T occurs when $J_z \gg 1$. We refer this phase to AFM(T). Note that, while the periods of both QLRO(T) and AFM(T) phase

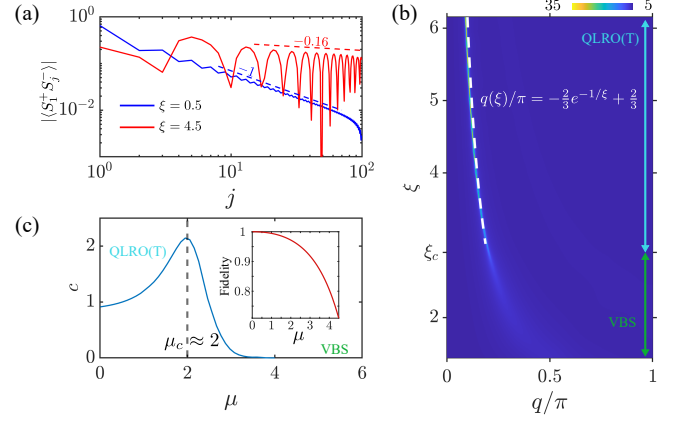


FIG. 4: (a) Spin correlation for $\xi = 0.5$ (blue solid line) and $\xi = 4.5$ (red solid line), which correspond respectively to the black square and circle in Fig. S3. The system size is $N = 100$. Dashed lines are fits $(j-1)^\eta$ with values of η being labeled beside each curve. (b) Static structure factor $S_{xy}(q)$ versus the momentum q and the interaction length ξ for $N = 300$. White dashed line is the fit $T(\xi) = 3/(1 - \exp(-1/\xi))$. The VBS-QLRO(T) phase transition point $\xi_c \approx 2.9$. (c) Central charge for Hamiltonian $H_{XX} = \sum_{m>n} J'(m-n) (S_m^+ S_n^- + S_n^+ S_m^-)$ with $\xi_0 = 4.5$. Inset shows the fidelity of two normalized bound states for different values of μ .

are controlled by interaction length, here the period of AFM(T) is commensurate [25].

Finally, we argue that the appearance of QLRO(T) and AFM(T) phases emerges from the strong frustration brought by the power-law factor of PLE interaction, which explains their absence in exponential and power-law decay interacting systems [25]. To identify our argument, we calculate the effective central charge for a system under long-range interaction $J'(x) = (\exp(-x/\xi_0) - \exp(-x/\xi_1)) / (\exp(-1/\xi_0) - \exp(-1/\xi_1))$ with ξ_0 chosen within QLRO(T) phase and $\xi_1 = \xi_0 - \mu$. The physical meaning of the parameter μ is clear. As the increase of μ , the interaction reduces to the superposition of two exponential decay components, therefore the frustration from power-law factor is destroyed. We present the phase diagram in Fig. S4(c). As expected, system undergoes a QLRO(T)-VBS phase transition when $\mu > \mu_c \approx 2$, which supports our above argument. At the transition point, the distinguishability between $J'(x)$ and PLE interaction with interaction length ξ_0 is approximate 0.97. Here we define the distinguishability of two kind of interactions $J_{1,2}(x)$ as the fidelity of two normalized dressed bound states $|\langle \varphi_1 | \varphi_2 \rangle|$ based on $J_1(x) \propto \langle x | \varphi_1 \rangle$ and $J_2(x) \propto \langle x | \varphi_2 \rangle$. This implies that the spiral phase only occurs when the interaction are highly overlapped with PLE interaction.

Discussion of experimental feasibility.—Regarding the experimental implementation of our proposal, the candidates include the system of color centers or cold atoms integrated into 1D photonics crystal waveguide [15, 33–

35], and the circuit QED system where the superconducting transmon qubits are coupled to an superconducting metamaterial waveguide [10, 36–38]. The photonic analog of SSH model has been experimentally realized both in photonic crystal waveguide [39–41] and superconducting metamaterials [42, 43]. As an example, let us choose the coupled circuit QED array to discuss the realization of the unconventional PLE interaction based on our proposal [25]. Specifically, the frequency of resonators on each site is equal and fixed by $\omega_0/2\pi = 10$ GHz. The nearest-neighbor intracell and intercell hopping strengths are fixed by $t_0/2\pi \approx 400$ MHz and $t_{-1}/2\pi \approx 113$ MHz, which can be controlled by the physical distance between neighboring resonators. The long-range hopping term beyond nearest-neighbor can be implemented by introducing additional capacitors, or by coupling lattice sites in groups to auxiliary cavities with time-dependent coupling strength followed by the adiabatic elimination of auxiliary cavities. In latter proposal, the undesired hopping terms can be greatly suppressed under the weak coupling approximation [11], therefore could barely affect the shape of PLE interaction. In circuit QED system, the weak qubit-photon coupling $\lambda/2\pi = 90$ MHz is realizable [44]. By coupling the qubit-photon bound state to external ports, one can probe the spatial distribution of dressed bound state (namely the d-d interaction) by measuring the coupling rate to the mode of external port [10]. In this design, we theoretically show that the PLE d-d interaction could be achieved even in the coupled-cavity array with small size $L = 20$ [25].

Conclusion.—In summary, we have shown how the PLE interaction emerges in a 1D waveguide QED system by appropriately designing the structure of lattice endowed with chiral symmetry. Applying the PLE interaction to a spin many-body model, we uncovered the exotic many-body phases in this system for the first time. Especially, we demonstrated the emergence of two spiral phases as the consequence of power-law factor for PLE interaction, which has no counterpart for other type of long-range interaction.

Besides those studied here, firstly, we expect our work could stimulate further studies for the unconventional long-range interactions by engineering the topological properties of photonic lattice. Secondly, our work demonstrates the topological waveguide QED system provides a platform of quantum simulation to discover novel complex phases of matter, which may further be explored beyond the XXZ model. Thirdly, it would be an interesting outlook to investigate how this kind of interaction affects the propagation of quantum information, namely the Lieb-Robinson bounds [45–47]. And lastly, it is worth studying the topological properties of PLE interacting system since long-range interaction could alter the topological intrinsicity of matters [48–51].

We thank Prof. Tao Shi for valuable discussions. This work is supported by the National Key Research and De-

velopment Program of China grant 2021YFA1400700.

* Electronic address: xinyoulu@hust.edu.cn

- [1] T. Giamarchi, *Quantum physics in one dimension*, Vol. 121 (Clarendon press, 2003).
- [2] S. Sachdev, *Quantum phase transitions* (Cambridge university press, 2011).
- [3] A. Auerbach, *Interacting electrons and quantum magnetism* (Springer Science & Business Media, 2012).
- [4] T. Dauxois, S. Ruffo, E. Arimondo, and M. Wilkens, in *Dynamics and thermodynamics of systems with long-range interactions* (Springer, 2002) pp. 1–19.
- [5] A. Campa, T. Dauxois, D. Fanelli, and S. Ruffo, *Physics of long-range interacting systems* (OUP Oxford, 2014).
- [6] A. Campa, T. Dauxois, and S. Ruffo, *Physics Reports* **480**, 57 (2009).
- [7] T. Lahaye, C. Menotti, L. Santos, M. Lewenstein, and T. Pfau, *Reports on Progress in Physics* **72**, 126401 (2009).
- [8] M. Saffman, T. G. Walker, and K. Mølmer, *Rev. Mod. Phys.* **82**, 2313 (2010).
- [9] N. Defenu, T. Donner, T. Macrì, G. Pagano, S. Ruffo, and A. Trombettoni, *Rev. Mod. Phys.* **95**, 035002 (2023).
- [10] E. Wigner, *Phys. Rev.* **46**, 1002 (1934).
- [11] N. D. Mermin and H. Wagner, *Phys. Rev. Lett.* **17**, 1133 (1966).
- [12] D. Vodola, L. Lepori, E. Ercolessi, and G. Pupillo, *New Journal of Physics* **18**, 015001 (2015).
- [13] M. F. Maghrebi, Z.-X. Gong, and A. V. Gorshkov, *Phys. Rev. Lett.* **119**, 023001 (2017).
- [14] S. John and J. Wang, *Phys. Rev. Lett.* **64**, 2418 (1990).
- [15] J. S. Douglas, H. Habibian, C.-L. Hung, A. V. Gorshkov, H. J. Kimble, and D. E. Chang, *Nature Photonics* **9**, 326 (2015).
- [16] G. Calajó, F. Ciccarello, D. Chang, and P. Rabl, *Phys. Rev. A* **93**, 033833 (2016).
- [17] M. T. Manzoni, L. Mathey, and D. E. Chang, *Nature communications* **8**, 1 (2017).
- [18] M. Bello, G. Platero, J. I. Cirac, and A. González-Tudela, *Science Advances* **5**, eaaw0297 (2019).
- [19] E. Kim, X. Zhang, V. S. Ferreira, J. Banker, J. K. Iverson, A. Sipahigil, M. Bello, A. González-Tudela, M. Mirhosseini, and O. Painter, *Phys. Rev. X* **11**, 011015 (2021).
- [20] L. Leonforte, A. Carollo, and F. Ciccarello, *Phys. Rev. Lett.* **126**, 063601 (2021).
- [21] W. Cheng, Z. Wang, and Y.-x. Liu, *Phys. Rev. A* **106**, 033522 (2022).
- [22] C. Vega, M. Bello, D. Porras, and A. González-Tudela, *Phys. Rev. A* **104**, 053522 (2021).
- [23] M. Bello, G. Platero, and A. González-Tudela, *PRX Quantum* **3**, 010336 (2022).
- [24] L. Leonforte, D. Valenti, B. Spagnolo, A. Carollo, and F. Ciccarello, *Nanophotonics* **10**, 4251 (2021).
- [25] See supplemental Material at URL for the proof of the connection between bound state and d-d interaction, exact solution of edge state, PLE interaction in higher dimensional lattice, the robustness of PLE interaction, PLE interaction with higher power-law exponent, more discussion about the many-body phases, and discussion

- about the experimental implementation of PLE interaction.
- [26] The PLE interaction implies $h(k) = (\exp(ik) - \exp(-1/\xi))^2 / \exp(ik)$. The band gap Δ_g equals to $2h(0)$. After some calculations one can obtain the expression in main text.
 - [27] U. L. Heras, A. Mezzacapo, L. Lamata, S. Filipp, A. Wallraff, and E. Solano, *Phys. Rev. Lett.* **112**, 200501 (2014).
 - [28] A. M. Childs, Y. Su, M. C. Tran, N. Wiebe, and S. Zhu, *Phys. Rev. X* **11**, 011020 (2021).
 - [29] M. Fishman, S. R. White, and E. M. Stoudenmire, “The ITensor software library for tensor network calculations,” (2020), [arXiv:2007.14822](https://arxiv.org/abs/2007.14822).
 - [9] P. Calabrese and J. Cardy, *Journal of Statistical Mechanics: Theory and Experiment* **2004**, P06002 (2004).
 - [31] C. K. Majumdar and D. K. Ghosh, *Journal of Mathematical Physics* **10**, 1388 (2003), https://pubs.aip.org/aip/jmp/article-pdf/10/8/1388/8804461/1388.1_online.pdf.
 - [32] A. W. Sandvik, *AIP Conference Proceedings* **1297**, 135 (2010).
 - [33] R. E. Evans, M. K. Bhaskar, D. D. Sukachev, C. T. Nguyen, A. Sipahigil, M. J. Burek, B. Machielse, G. H. Zhang, A. S. Zibrov, E. Bielejec, H. Park, M. Lončar, and M. D. Lukin, *Science* **362**, 662 (2018).
 - [34] A. Sipahigil, R. E. Evans, D. D. Sukachev, M. J. Burek, J. Borregaard, M. K. Bhaskar, C. T. Nguyen, J. L. Pacheco, H. A. Atikian, C. Meuwly, R. M. Camacho, F. Jelezko, E. Bielejec, H. Park, M. Lončar, and M. D. Lukin, *Science* **354**, 847 (2016).
 - [35] S. Barik, A. Karasahin, C. Flower, T. Cai, H. Miyake, W. DeGottardi, M. Hafezi, and E. Waks, *Science* **359**, 666 (2018).
 - [36] T. Ozawa, H. M. Price, A. Amo, N. Goldman, M. Hafezi, L. Lu, M. C. Rechtsman, D. Schuster, J. Simon, O. Zeitner, and I. Carusotto, *Rev. Mod. Phys.* **91**, 015006 (2019).
 - [37] P. Lodahl, S. Mahmoodian, and S. Stobbe, *Rev. Mod. Phys.* **87**, 347 (2015).
 - [38] D. E. Chang, J. S. Douglas, A. González-Tudela, C.-L. Hung, and H. J. Kimble, *Rev. Mod. Phys.* **90**, 031002 (2018).
 - [39] R. Keil, J. M. Zeuner, F. Dreisow, M. Heinrich, A. Tünnermann, S. Nolte, and A. Szameit, *Nature communications* **4**, 1368 (2013).
 - [40] M. Xiao, Z. Q. Zhang, and C. T. Chan, *Phys. Rev. X* **4**, 021017 (2014).
 - [41] X.-D. Chen, D. Zhao, X.-S. Zhu, F.-L. Shi, H. Liu, J.-C. Lu, M. Chen, and J.-W. Dong, *Phys. Rev. A* **97**, 013831 (2018).
 - [42] C. H. Lee, S. Imhof, C. Berger, F. Bayer, J. Brehm, L. W. Molenkamp, T. Kiessling, and R. Thomale, *Communications Physics* **1**, 39 (2018).
 - [43] T. Goren, K. Plekhanov, F. Appas, and K. Le Hur, *Phys. Rev. B* **97**, 041106 (2018).
 - [44] Y. Liu and A. A. Houck, *Nature Physics* **13**, 48 (2017).
 - [45] P. Hauke and L. Tagliacozzo, *Phys. Rev. Lett.* **111**, 207202 (2013).
 - [46] P. Richerme, Z.-X. Gong, A. Lee, C. Senko, J. Smith, M. Foss-Feig, S. Michalakis, A. V. Gorshkov, and C. Monroe, *Nature* **511**, 198 (2014).
 - [47] P. Jurcevic, B. P. Lanyon, P. Hauke, C. Hempel, P. Zoller, R. Blatt, and C. F. Roos, *Nature* **511**, 202 (2014).
 - [48] D. Vodola, L. Lepori, E. Ercolessi, A. V. Gorshkov, and G. Pupillo, *Phys. Rev. Lett.* **113**, 156402 (2014).
 - [49] K. Patrick, T. Neupert, and J. K. Pachos, *Phys. Rev. Lett.* **118**, 267002 (2017).
 - [50] Z. Gong, T. Guaita, and J. I. Cirac, *Phys. Rev. Lett.* **130**, 070401 (2023).
 - [51] N. G. Jones, R. Thorngren, and R. Verresen, *Phys. Rev. Lett.* **130**, 246601 (2023).

Supplemental Material for “Power-Law-Exponential Interaction Induced Quantum Spiral Phases”

This supplement material contains seven parts: I. A detail proof for the connection between the dressed bound state and dipole-dipole (d-d) interactions in waveguide QED; II. The exact solution of the zero-energy edge state; III. The discussion on the realization of similar PLE interaction in higher dimensional lattice; IV. A additional discussion about the robustness of the PLE interactions against disorder; V. Realizing PLE interaction with higher power-law exponent; VI. A detailed discussion of the spin many-body phases; VII. A detailed discussion of the experimental implementation of PLE interaction.

Contents

I. Proof for the connection between bound state and d-d interactions	1
A. Exact dynamics of two quantum emitters (QEs) coupled to a structured bosonic bath	1
B. Connection between bath GF and d-d interactions	3
C. Connection between bath GF and the dressed bound state	5
II. Exact solution of the Edge state	6
A. Edge state with chirality	6
B. Edge state without chirality	8
III. Power-law enhanced interaction in higher dimensional lattice	9
IV. Topological protection of PLE interaction	10
V. PLE interaction with the higher power-law exponent	12
VI. Further discussion about the many-body phases	12
A. FM phase and its boundary	12
B. Other phase boundaries	14
VII. Discussion of experimental implementation of PLE interaction	14
References	15

I. PROOF FOR THE CONNECTION BETWEEN BOUND STATE AND D-D INTERACTIONS

In this section, by exploring the system dynamics, we provide the detailed proof of the connection between dressed bound state and d-d interaction in the generic waveguide QED system under the Markovian approximation, i.e., $J(x) \propto \lambda \phi(x)$ where $\phi(x)$ is the real-space component of dressed bound state.

A. Exact dynamics of two quantum emitters (QEs) coupled to a structured bosonic bath

Under the frame of generic waveguide QED systems, the Hamiltonian that describes two QEs coupling to a bosonic bath reads as

$$H_2 = H_s + H_b + V = \omega_q \sum_{j=1}^2 \sigma_j^\dagger \sigma_j + H_b + \lambda \sum_{j=1}^2 (a_{x_{j,\alpha}}^\dagger \sigma_j + h.c.), \quad (S1)$$

where $a_{x_{j,\alpha}}$ denotes the annihilation operator at the position $x_{j,\alpha}$ of bath. Without loss of generality, we assume that the spectrum of H_b possesses energy band structure, such that $a_{x_{j,\alpha}}$ could be sublattice-dependent (cf. the bath we considered in main text where $a_{x_{j,\alpha}} \in \{a_{x_{j,A}}, a_{x_{j,B}}\}$). To obtain the analytical results, we assume the

thermaldynamical limit of bath in the following derivations. Then the time-evolution operator of system can be obtained by the Inverse-Fourier transform of the Green's function (GF) [1]

$$U(t) = e^{-itH_2} = \frac{1}{2\pi i} \int_C G_2(z) e^{-izt} dz = \frac{1}{2\pi i} \int_C \frac{1}{z - H_2} e^{-izt} dz, \quad (S2)$$

where the integral contour is shown in Fig. S1. The single-excitation dynamic of QEs is obtained by projecting $U(t)$ onto the QEs subspace, which leads to

$$PU(t)P = \frac{1}{2\pi i} \int_C PG_2(z)P e^{-izt} dz. \quad (S3)$$

Here the operators $P = \sum_{i=1}^2 |e_i, 0\rangle\langle e_i, 0|$ and $Q = \sum_{j,\alpha} a_{x_{j,\alpha}}^\dagger |g, 0\rangle\langle g, 0| a_{x_{j,\alpha}}$ ($P + Q = \mathbb{I}_1$) are the projectors onto the QEs and the bath subspace in the single-excitation regime, respectively. The projected GF has the form $PG(z)P = P[z - H_s - R(z)]^{-1}P$ where $R(z) = V + VQ(z - QH_2Q)^{-1}V$ is the level-shift operator, and the projected level-shift operator $PR(z)P$ is

$$PR(z)P = PVP + PV \frac{Q}{z - QH_2Q} VP = PV \frac{Q}{z - H_b} VP = PVG_b(z)VP. \quad (S4)$$

The first equal holds since V is zero matrix in the QEs and bath subspace, i.e., $PVP = QVQ = 0$. Here $G_b(z) = Q(z - H_b)^{-1}Q$ is the single-particle GF of bath [2]. Inserting Eq. (S4) and V into the projected GF, we have

$$PG_2(z)P = \frac{1}{\det G_2(z)} (|e_1, 0\rangle \quad |e_2, 0\rangle) \begin{pmatrix} z - \omega_q - \lambda^2 G_b(x_{2,\beta}, x_{2,\beta}; z) & \lambda^2 G_b(x_{2,\beta}, x_{1,\alpha}; z) \\ \lambda^2 G_b(x_{1,\alpha}, x_{2,\beta}; z) & z - \omega_q - \lambda^2 G_b(x_{1,\alpha}, x_{1,\alpha}; z) \end{pmatrix} \begin{pmatrix} \langle e_1, 0| \\ \langle e_2, 0| \end{pmatrix} \quad (S5)$$

with

$$\det G_2(z) = (z - \omega_q - \lambda^2 G_b(x_{1,\alpha}, x_{1,\alpha}; z))(z - \omega_q - \lambda^2 G_b(x_{2,\beta}, x_{2,\beta}; z)) - \lambda^4 G_b(x_{1,\alpha}, x_{2,\beta}; z)G_b(x_{2,\beta}, x_{1,\alpha}; z), \quad (S6)$$

where $G_b(x_{i,\alpha}, x_{j,\beta}; z) = \langle 0|a_{x_{i,\alpha}}(z - H_b)^{-1}a_{x_{j,\beta}}^\dagger|0\rangle$ denotes single-particle bath GF in real space. Under these notations, the projected evolution operator in Eq. (S3) is given by

$$PU(t)P = \frac{1}{2\pi i} \int_C dz \frac{e^{-izt}}{\det G_2(z)} (|e_1, 0\rangle \quad |e_2, 0\rangle) \begin{pmatrix} z - \omega_q - \lambda^2 G_b(x_{2,\beta}, x_{2,\beta}; z) & \lambda^2 G_b(x_{2,\beta}, x_{1,\alpha}; z) \\ \lambda^2 G_b(x_{1,\alpha}, x_{2,\beta}; z) & z - \omega_q - \lambda^2 G_b(x_{1,\alpha}, x_{1,\alpha}; z) \end{pmatrix} \begin{pmatrix} \langle e_1, 0| \\ \langle e_2, 0| \end{pmatrix}. \quad (S7)$$

Now let us assume that the system is prepared in the initial state $|\psi(0)\rangle = |e_1, 0\rangle$. According to Eq. (S7), the t time probability amplitude of system state $|e_2, 0\rangle$ is given by

$$c_2(t) = \langle e_2, 0|PU(t)P|e_1, 0\rangle = \frac{1}{2\pi i} \int_C \frac{\lambda^2 G_b(x_{1,\alpha}, x_{2,\beta}; z)}{\det G_2(z)} e^{-izt} dz. \quad (S8)$$

To calculate this integral, we need to close the contour in the lower half complex plane, which leads to [3]

$$c_2(t) = \sum_{z_k \in \text{BSEs}} \text{Res}(z_k) e^{-iz_k t} + \sum_{z_k \in \text{UPs}} \text{Res}(z_k) e^{-iz_k t} - \sum_{m \in \text{BCDs}} C_m(t). \quad (S9)$$

Here $\text{Res}(z_i)$ are the residues corresponding to the integrand at z_i . The full dynamics is decomposed into three parts: (i) The bound state contributions from the real poles; (ii) The unstable pole contributions from the poles with negative image part; (iii) The branch cut detours contributions from the branch cuts introduced by bath Green's function $G_b(z)$. The contributions from unstable poles and branch cut detours decays with time, and thus only the bound state contributions survival in the long-time limit $t \gg 1/\lambda$, i.e.,

$$\lim_{t \gg 1/\lambda} c_2(t) = \sum_{z_k \in \text{BSEs}} \text{Res}(z_k) e^{-iz_k t}. \quad (S10)$$

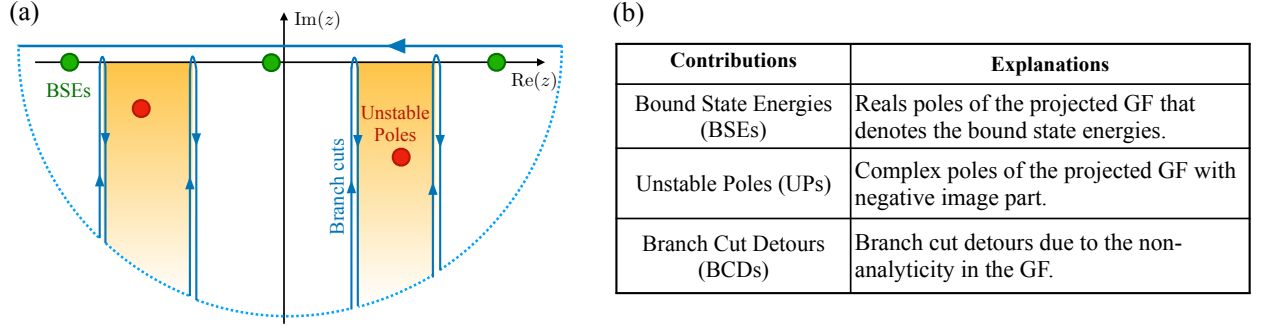


FIG. S1: (a) Example of an integration contour (horizontal blue line) to calculate Eq. (S2). One needs to close the contour in the lower complex plane (dashed and vertical blue line) to carry out the integration. Thus the time-evolutions of QEs is fully described by three part of contributions. (b) Explanations of the contributions to the dynamics of QEs.

B. Connection between bath GF and d-d interactions

In order to get a full description of QEs coherent dynamics, we need to find the poles of the integrand in Eq. (S8) in band-gap regime (namely the BSEs) by solving the poles equation

$$\det G_2(E_i) = (E_i - \omega_q - \lambda^2 G_b(x_{1,\alpha}, x_{1,\alpha}; E_i))(E_i - \omega_q - \lambda^2 G_b(x_{2,\beta}, x_{2,\beta}; E_i)) - \lambda^4 |G_b(x_{1,\alpha}, x_{2,\beta}; E_i)|^2 = 0. \quad (\text{S11})$$

Before proceeding, we turn to the dynamics of single QE system with Hamiltonian $H_1 = \omega_q \sigma_1^\dagger \sigma_1 + H_b + \lambda(a_{x_{1,\alpha}}^\dagger \sigma_1 + h.c.)$. The projected GF and related poles equation are now

$$P G_1(z) P = \frac{|e, 0\rangle\langle e, 0|}{\det G_1(z)} \quad \text{and} \quad \det G_1(E_k) = E_k - \omega_q - \lambda^2 G_b(x_{1,\alpha}, x_{1,\alpha}; E_k) = 0. \quad (\text{S12})$$

Solving the poles equation, one can get the BSEs of H_1 denoted by $\{E_1, E_2, \dots, E_q, \dots, E_m\}$, where the special BSE E_q represents the eigenvalue closed to ω_q [see Fig. S2]. Given these poles, the corresponding residues are

$$\text{Res}(E_k) = \frac{1}{\frac{d}{dz} \det G_1(z)|_{z=E_k}} = \frac{1}{1 + \lambda^2 \langle 0 | a_{x_{1,\alpha}} (E_k - H_b)^{-2} a_{x_{1,\alpha}}^\dagger | 0 \rangle}, \quad (\text{S13})$$

where $\langle 0 | a_{x_{1,\alpha}} (E_k - H_b)^{-2} a_{x_{1,\alpha}}^\dagger | 0 \rangle = -\frac{d}{dz} G_b(x_{1,\alpha}, x_{1,\alpha}; z)|_{z=E_k}$. As shown in the following discussion, only few residues in Eq. (S13) have non-negligible contributions for the dynamics of QE. First of all, there is at most one solution of Eq. (S12), namely BSE, within each band-gap regime [4, 5]. The corresponding GFs at these BSEs yield

$$|G_b(x_{1,\alpha}, x_{1,\alpha}; E_q) - G_b(x_{1,\alpha}, x_{1,\alpha}; E_i \neq E_q)| = \frac{|E_q - E_i|}{\lambda^2} > \frac{\min\{\Delta_{\text{band}}\}}{\lambda^2}. \quad (\text{S14})$$

Secondly, the term of $\min\{\Delta_{\text{band}}\}/\lambda^2$ implies $|G_b(x_{1,\alpha}, x_{1,\alpha}; E_i \neq E_q) - G_b(x_{1,\alpha}, x_{1,\alpha}; E_q)| \sim \mathcal{O}(\lambda^{-2})$. Under Markovian approximation (where λ is sufficiently weak), the differences of GFs at two BSE will take large value, which is only satisfied when E_i is closed to the band-edge due to the monotonicity of $G_b(x_{1,\alpha}, x_{1,\alpha}; z)$. The distribution of BSEs eventually leads to a generic relation for the residues

$$\text{Res}(E_q) = \left(1 + \lambda^2 \langle 0 | a_{x_{1,\alpha}} (E_q - H_b)^{-2} a_{x_{1,\alpha}}^\dagger | 0 \rangle\right)^{-1} \gg \text{Res}(E_i \neq E_q) = \left(1 + \lambda^2 \langle 0 | a_{x_{1,\alpha}} (E_i - H_b)^{-2} a_{x_{1,\alpha}}^\dagger | 0 \rangle\right)^{-1}. \quad (\text{S15})$$

The approximation holds since the derivation $dG_b(x_{1,\alpha}, x_{1,\alpha}; z)/dz$ has a divergence for E_i near the band-edge in one- and two-dimensional baths with tight-binding and quadratic dispersions [4]. Thus, our previous and following derivation applies to these baths. Combined with Eq. (S9), we finally obtain an approximate expression of the single QE long-time dynamics as

$$c_1(t) \approx \text{Res}(E_q) e^{-iE_q t} = \frac{e^{-iE_q t}}{1 + \lambda^2 \langle 0 | a_{x_{1,\alpha}} (E_q - H_b)^{-2} a_{x_{1,\alpha}}^\dagger | 0 \rangle}, \quad (\text{S16})$$

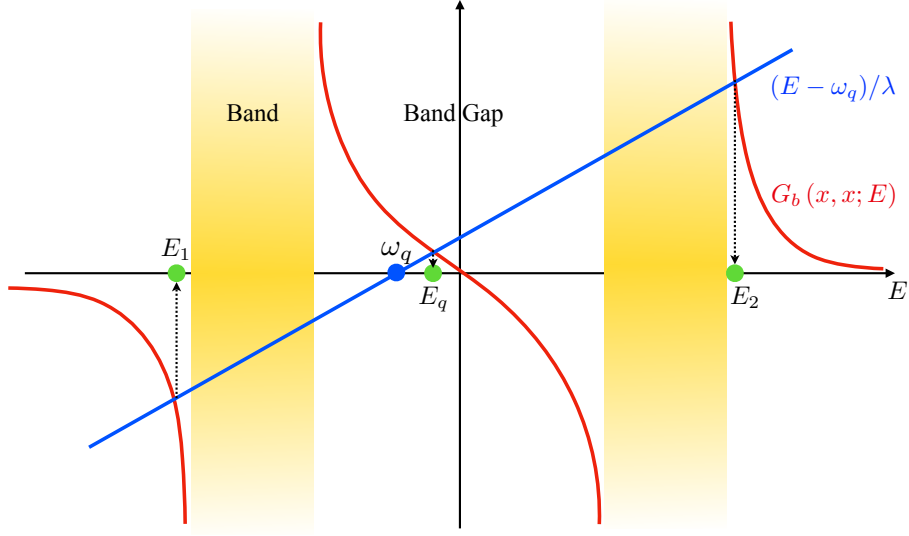


FIG. S2: A typical GF versus E (red line) for a 1D bath with two bands. Roots of the poles equation (i.e., the BSEs) are obtained from the intersections of two lines. GFs for 1D bath and the associated derivations are divergent at each band edge, while could be convergent for higher-dimensional bath.

which is a constant for the probability $|c_1(t)|^2 \approx |\text{Res}(E_q)|^2$.

Now let's return to the long-time behavior of two QEs system. In order to obtain an dynamics governed by d-d interaction, the energy corrections induced by the bath for each atom should be equal, such that the bath GF obeys $G_b(x_{j,\alpha}, x_{j,\alpha}; z) = G_b(x_{j,\beta}, x_{j,\beta}; z)$ for $\alpha \neq \beta$. Noting that, the only difference in poles equations between Eq. (S11) and Eq. (S12) are the extra terms $\pm \lambda^2 |G_b(x_{1,\alpha}, x_{2,\beta}; E_i)|$. Under Markovian approximation, we perform a perturbation expansion to poles equation $\det G_2(z) = 0$ at $z = E_q$ up to the first order of $\delta E = E - E_q$, and obtain

$$\delta E - \delta E \lambda^2 \frac{dG_b(x_{1,\alpha}, x_{1,\alpha}; z)}{dz} \Big|_{E_q} = \pm \lambda^2 \left| G_b(x_{1,\alpha}, x_{2,\beta}; E_q) + \delta E \frac{dG_b(x_{1,\alpha}, x_{2,\beta}; z)}{dz} \Big|_{E_q} \right| \approx \pm \lambda^2 |G_b(x_{1,\alpha}, x_{2,\beta}; E_q)|. \quad (\text{S17})$$

Solving this equation results in

$$\delta E_q \approx \pm \lambda^2 \frac{|G_b(x_{1,\alpha}, x_{2,\beta}; E_q)|}{1 + \lambda^2 \langle 0 | a_{x_{1,\alpha}} (E_q - H_b)^{-2} a_{x_{1,\alpha}}^\dagger | 0 \rangle}. \quad (\text{S18})$$

Inserting the approximate solution $E_q^\pm \approx E_q + \delta E_q$ into Eq. (S10), the coherent dynamics is now approximately given by

$$c_2(t) \approx \text{Res}(E_q^+) e^{-iE_q^+ t} + \text{Res}(E_q^-) e^{-iE_q^- t} \quad (\text{S19})$$

with the corresponding residues

$$\begin{aligned} \text{Res}(E_q^\pm) &= \lim_{z \rightarrow E_q^\pm} \frac{\lambda^2 G_b(x_{1,\alpha}, x_{2,\beta}; z)}{\frac{d}{dz} [(z - \omega_q - \lambda^2 G_b(x_{1,\alpha}, x_{1,\alpha}; z))^2 - \lambda^4 G_B(x_{1,\alpha}, x_{2,\beta}; z) G_B(x_{2,\beta}, x_{1,\alpha}; z)]} \\ &= \frac{1}{\pm \left(1 + \lambda^2 \langle 0 | a_{x_{1,\alpha}} (E_q - H_b)^{-2} a_{x_{1,\alpha}}^\dagger | 0 \rangle \right) - \lambda^2 \left(\langle 0 | a_{x_{1,\alpha}} (E_q - H_b)^{-2} a_{x_{2,\beta}}^\dagger | 0 \rangle e^{i\theta(E_q^\pm)} + c.c. \right)} \frac{e^{i\theta(E_q^\pm)}}{2} \quad (\text{S20}) \\ &\approx \frac{1}{\pm \left(1 + \lambda^2 \langle 0 | a_{x_{1,\alpha}} (E_q - H_b)^{-2} a_{x_{1,\alpha}}^\dagger | 0 \rangle \right) - \lambda^2 \left(\langle 0 | a_{x_{1,\alpha}} (E_q - H_b)^{-2} a_{x_{2,\beta}}^\dagger | 0 \rangle e^{i\theta(E_q)} + c.c. \right)} \frac{e^{i\theta(E_q)}}{2}, \end{aligned}$$

where $\theta(z) = \arg \{G_b(x_{1,\alpha}, x_{2,\beta}; z)\}$. Then substituting Eqs. (S18, S20) in Eq. (S19), we have

$$c_2(t) \approx \text{Res}(E_q^+) e^{-i(E_q + |\delta E_q|)t} + \text{Res}(E_q^-) e^{-i(E_q - |\delta E_q|)t}. \quad (\text{S21})$$

As for the expression of $c_1(t)$, one just need to replace the numerator $\lambda^2 G_b(x_{1,\alpha}, x_{2,\beta}; z)$ of Eq. (S20) with $z - \omega_q - \lambda^2 G_b(x_{1,\alpha}, x_{1,\alpha}; z)$, which returns to $\pm \lambda^2 |G_b(x_{1,\alpha}, x_{2,\beta}; z)|$ for real z . The sign is fixed by the fact that $z - \omega_q - \lambda^2 G_b(x_{1,\alpha}, x_{1,\alpha}; z)$ have respectively (+) and (-) sign at $z = E_q^+$ and $z = E_q^-$, due to the monotonicity of $G_b(x_{1,\alpha}, x_{1,\alpha}; z)$ and the zero at E_q . After some algebras, we have

$$c_1(t) \approx \text{Res}'(E_q^+) e^{-i(E_q + |\delta E_q|)t} + \text{Res}'(E_q^-) e^{-i(E_q - |\delta E_q|)t}, \quad (\text{S22})$$

where

$$\text{Res}'(E_q^\pm) = \frac{\pm 1}{\pm \left(1 + \lambda^2 \langle 0 | a_{x_{1,\alpha}} (E_q - H_b)^{-2} a_{x_{1,\alpha}}^\dagger | 0 \rangle\right) - \lambda^2 \left(\langle 0 | a_{x_{1,\alpha}} (E_q - H_b)^{-2} a_{x_{2,\beta}}^\dagger | 0 \rangle e^{i\theta(E_q)} + c.c.\right)} \frac{1}{2}. \quad (\text{S23})$$

Under Markovian limit, $\text{Res}(E_q^\pm)$ converge to $\pm e^{i\theta(E_q)}/2$ and $\text{Res}'(E_q^\pm)$ converge to $1/2$ along with the terms proportional to λ^2 approaching to zero. This leads to

$$c_1(t) \approx \left[e^{-i(E_q + |\delta E_q|)t} + e^{-i(E_q - |\delta E_q|)t} \right] / 2, \quad c_2(t) \approx \left[e^{-i(E_q + |\delta E_q|)t} - e^{-i(E_q - |\delta E_q|)t} \right] \frac{e^{i\theta(E_q)}}{2}. \quad (\text{S24})$$

Now, let's consider the dynamics governed by an effective d-d Hamiltonian $H_{\text{eff}} = \sum_{m=1}^2 \omega \sigma_m^+ \sigma_m^- + J^* \sigma_1^+ \sigma_2^- + J \sigma_1^- \sigma_2^+$ with $J = |J|e^{i\theta}$, and we obtain

$$\langle e_1 | e^{-iH_{\text{eff}}t} | e_1 \rangle = \left[e^{-i(\omega + |J|)t} + e^{-i(\omega - |J|)t} \right] / 2, \quad \langle e_2 | e^{-iH_{\text{eff}}t} | e_1 \rangle = \left[e^{-i(\omega + |J|)t} - e^{-i(\omega - |J|)t} \right] \frac{e^{i\theta}}{2}. \quad (\text{S25})$$

Comparing Eq. (S24) to Eq. (S25), we conclude that the dynamics of QEs can be approximately interpreted as the coherent d-d dynamics, with the effective Hamiltonian H_{eff} given by

$$H_{\text{eff}} = \begin{pmatrix} E_q & |\delta E_q| e^{-i\theta(E_q)} \\ |\delta E_q| e^{i\theta(E_q)} & E_q \end{pmatrix}. \quad (\text{S26})$$

Accordingly, the d-d interaction mediated by bath can be expressed as the bath GF at E_q , i.e.,

$$J(x_{1,\alpha}, x_{2,\beta}) \approx |\delta E_q| e^{i\theta(E_q)} \approx \eta^{-1} \lambda^2 G_b(x_{1,\alpha}, x_{2,\beta}; E_q), \quad (\text{S27})$$

where the real correction factor $\eta = 1 + \lambda^2 \langle 0 | a_{x_{1,\alpha}} (E_q - H_b)^{-2} a_{x_{1,\alpha}}^\dagger | 0 \rangle \geq 1$.

C. Connection between bath GF and the dressed bound state

Let us project the single QE system GF on bath subspace by [1]

$$QG(z)Q = \frac{Q}{z - QH_1Q} + \frac{Q}{z - QH_1Q} VPG(z)PV \frac{Q}{z - QH_1Q} = G_b(z) + G_b(z)VPG(z)PVG_b(z). \quad (\text{S28})$$

Then, we have

$$\langle 0 | a_{x_{2,\beta}} QG(z)Q a_{x_{2,\beta}}^\dagger | 0 \rangle = G_b(x_{2,\beta}, x_{2,\beta}; z) + \lambda^2 \frac{G_b(x_{1,\alpha}, x_{2,\beta}; z) G_b(x_{2,\beta}, x_{1,\alpha}; z)}{z - \omega_q - \lambda^2 G_b(x_{1,\alpha}, x_{1,\alpha}; z)}. \quad (\text{S29})$$

Since this expression has a pole at $z = E_q$, a tiny cycle integral around E_q is performed to carry out the residue, which gives nothing but the dressed bound state component $|\phi\rangle$ with eigenvalue E_q as

$$\oint_{E_q} \langle 0 | a_{x_{2,\beta}} QG(z)Q a_{x_{2,\beta}}^\dagger | 0 \rangle dz = 2\pi i |\langle 0 | a_{x_{2,\beta}} | \phi \rangle|^2 = \frac{2\pi i}{\eta} \lambda^2 |G_b(x_{1,\alpha}, x_{2,\beta}; E_q)|^2. \quad (\text{S30})$$

This expression gives the relation between the dressed bound state and GFs, which is

$$\langle 0 | a_{x_{2,\beta}} | \phi \rangle = \sqrt{\eta^{-1}} \lambda G_b(x_{1,\alpha}, x_{2,\beta}; E_q). \quad (\text{S31})$$

Combining with Eq. (S27), we finally prove the connection between dressed bound state and d-d interaction, as

$$J(x_{1,\alpha}, x_{2,\beta}) \approx \eta^{-1/2} \lambda \langle 0 | a_{x_{2,\beta}} | \phi \rangle. \quad (\text{S32})$$

For the system we considered in main text, the bath Hamiltonian respects chiral symmetry that induces the symmetric spectrum around the bare frequency of bath modes ω_0 . Under the resonance condition, vacancy-like dressed state ensures that $E_q = \omega_0$ and $|\phi\rangle = |\varphi_E\rangle$ ($|\varphi_E\rangle$ is the edge state of bath), and thus $J(x_{1,\alpha}, x_{2,\beta}) \approx \eta^{-1/2} \lambda \langle 0 | a_{x_{2,\beta}} | \varphi_E \rangle$.

II. EXACT SOLUTION OF THE EDGE STATE

To support the analytical PLE d-d interactions given in Eq. (2) of the main text, we provide the detailed derivation for the chiral edge state of bath in subsection A. We also show how to implement nonchiral edge state in subsection B to support the interaction used in the simulation of many-body phase.

A. Edge state with chirality

Our goal is to solve the eigenequation in real space

$$[H_b + \epsilon |x_{1,A}\rangle\langle x_{1,A}|] |\varphi_E\rangle = 0 |\varphi_E\rangle, \quad (\text{S33})$$

where $\epsilon = \lambda^2/(E_q - \omega_q) \rightarrow \infty$ for $E_q = \omega_q = \omega_0 = 0$ is the effective potential induced by the QE. Inserting $H_b = d_x(k)\sigma_x + d_y(k)\sigma_y$ into this equation, we have

$$\sum_q \left[\sum_m^P t_{-m} \langle (q-m)_B | \varphi_E \rangle + \sum_n^Q t_{+n} \langle (q+n)_B | \varphi_E \rangle + \epsilon \delta_{q,x_1} \langle q_A | \varphi_E \rangle \right] = 0, \quad (\text{S34a})$$

$$\sum_q \left[\sum_m^P t_{-m}^* \langle (q+m)_A | \varphi_E \rangle + \sum_n^Q t_{+n}^* \langle (q-n)_A | \varphi_E \rangle \right] = 0, \quad (\text{S34b})$$

where $q \in \mathbb{Z}$ is the cell index. To solve this difference equation, we perform a Z-Transform, and obtain

$$h(z)\Phi_B(z) + \epsilon \langle x_{1,A} | \varphi_E \rangle = \left(\sum_m^P t_{-m} z^{-m} + \sum_n^Q t_{+n} z^n \right) \Phi_B(z) + \epsilon \langle x_{1,A} | \varphi_E \rangle z^{-x_{1,A}} = 0, \quad (\text{S35a})$$

$$h^*(z^{-1})\Phi_A(z) = \left(\sum_m^P t_{-m}^* z^m + \sum_n^Q t_{+n}^* z^{-n} \right) \Phi_A(z) = 0. \quad (\text{S35b})$$

One immediate result is $\Phi_A(z) = 0$, which implies that the edge state component on sublattice A vanishes. The expression of $h(z)$ can be rewritten as a compact form $h(z) = f(z)/g(z)$ with $f(z) = \sum_m^P t_{-m} z^{-m} + \sum_n^Q t_{+n} z^{P+n}$ and $g(z) = z^P$. Then, the component on sublattice B can be carried out by the Inverse Z-Transform, which reads as

$$\langle x_{2,B} | \varphi_E \rangle = \frac{1}{2\pi i} \oint_{|z|=1} z^{x_{2,B}-x_{1,A}-1} \Phi_B(z) dz = \frac{-\epsilon \langle x_{1,A} | \varphi_E \rangle}{2\pi i} \oint_{|z|=1} \frac{z^{x+P-1}}{f(z)} dz, \quad (\text{S36})$$

where we define $x = x_{2,B} - x_{1,A}$ as the relative distance. According to the *Fundamental Theorem of Algebra*, $f(z)$ can be factored as $f(z) = \prod_{\mu=1}^{P+W} (z - z_\mu) \prod_{\nu=P+W+1}^{P+Q} (z - z_\nu)$. Here we firstly assume that all $P+Q$ zeros of $f(z)$ are distinctive, i.e. $z_i \neq z_j$ for $i \neq j$. The index μ (ν) labels the zeros of $f(z)$ inside (outside) the unit circle in complex plane. The number of zeros inside (outside) the complex plane is given by $P+W$ ($Q-W$). This can be identified by recalling the definition of winding number $W = n_{\text{zeros}} - n_{\text{poles}}$, where n_{zeros} (n_{poles}) is the number of zeros (poles) of $h(z)$ inside the unit circle. In our case, n_{zeros} equals to the number of zeros of $f(z)$ inside the unit circle and $n_{\text{poles}} = P$, thus the number of zeros of $f(z)$ inside the unit circle $n_{\text{zeros}} = W + n_{\text{poles}} = W + P$ and the number of zeros of $f(z)$ outside the unit circle equals to $P+Q - n_{\text{zeros}}$ that gives $Q-W$. Then one can use residue theorem to integrate out Eq. (S36). Let $x_c = 1 - P$, the normalized edge state can be expressed as

$$\langle x | \varphi_E \rangle = \frac{1}{\mathcal{N}} \left(\sum_{\mu=1}^{P+W} \text{Res} \left[\frac{z_\mu^{x-x_c}}{f(z_\mu)} \right] + \text{Res} \left[\frac{0^{x-x_c}}{f(0)} \right] \right), \quad (\text{S37})$$

where \mathcal{N} is the normalized constant. This formula can be further evaluated as

$$\langle x | \varphi_E \rangle = \frac{1}{\mathcal{N}} \left\{ \sum_{\mu=1}^{P+W} \text{Res} \left[\frac{z_\mu^{x-x_c}}{f(z_\mu)} \right] + \text{Res} \left[\frac{0^{x-x_c}}{f(0)} \right] = \sum_{\mu=1}^{P+W} \frac{e^{-(x-x_c)/\xi_\mu}}{\prod_{\alpha \neq \mu} (z_\mu - z_\alpha)} \right. \\ \left. \sum_{\mu=1}^{P+W} \text{Res} \left[\frac{z_\mu^{x-x_c}}{f(z_\mu)} \right] + \text{Res} \left[\frac{0^{x-x_c}}{f(0)} \right] = \sum_{\nu=P+W+1}^{P+Q} -\text{Res} \left[\frac{z_\nu^{x-x_c}}{f(z_\nu)} \right] = \sum_{\nu=P+W+1}^{P+Q} \frac{-e^{-(x-x_c)/\xi_\nu}}{\prod_{\beta \neq \nu} (z_\nu - z_\beta)} \right\}. \quad (\text{S38})$$

The upper (bottom) line holds for $x \geq x_c$ ($x < x_c$). From this formula, it's clear that the obtained interaction is the superposition of exponential decay components with the different decay length $\xi_{\mu,\nu} = -1/\ln(z_{\mu,\nu})$, and the number of components involving superposition is $P + W$ ($Q - W$) for $x \geq x_c$ ($x < x_c$). Now we are in the position to derive the PLE interaction from Eq. (S38). To this end, consider that n out of $P + W$ zeros inside the unit circle coincide with z_p , namely a higher-order zero z_p with order n in $f(z)$. Then, the superposition of these n components with the same decay length $\xi_p = -1/\ln(z_p)$ reduces to

$$\lim_{z_{i_1}, z_{i_2}, \dots, z_{i_n} \rightarrow z_p} \sum_{\mu=1}^n \frac{e^{-(x-x_c)/\xi_{i_\mu}}}{\prod_{i_\alpha \neq i_\mu} (z_{i_\mu} - z_{i_\alpha}) \prod_{\alpha' \neq \{i_1, \dots, i_n\}} (z_{i_\mu} - z_{\alpha'})}. \quad (\text{S39})$$

To carry out this limitation, let $z_{i_1} = z_p + h$, $z_{i_2} = z_p + 2h, \dots, z_{i_n} = z_p + nh$ and we have

$$\lim_{h \rightarrow 0} \sum_{\mu=1}^n \frac{1}{\prod_{\alpha' \neq \{i_1, \dots, i_n\}} (z_{i_\mu} - z_{\alpha'})} \frac{(-1)^{n-\mu} (z_p + \mu h)^{x-x_c}}{(\mu-1)!(n-\mu)! h^{n-1}} \propto \lim_{h \rightarrow 0} \frac{1}{h^{n-1}} \sum_{s=0}^{n-1} \sum_{\mu=1}^n \frac{(-1)^{n-\mu} z_p^{x-x_c} \binom{x-x_c}{s} h^s / z_p^s}{(\mu-1)!(n-\mu)!} + \mathcal{O}(h). \quad (\text{S40})$$

The summation over μ gives

$$\sum_{\mu=1}^n \frac{(-1)^{n-\mu} z_p^{x-x_c} \binom{x-x_c}{s} h^s / z_p^s}{(\mu-1)!(n-\mu)!} = h^s z_p^{x-x_c-s} \binom{x-x_c}{s} S_2(s+1, n), \quad (\text{S41})$$

where $S_2(\bullet, \bullet)$ is the Stirling number of the second kind. The right-hand-side of this equation gives 0 for $s \neq n-1$ and $h^s z_p^{x-x_c-s} \binom{x-x_c}{s}$ for $s = n-1$. Therefore, the limitation in the right-hand-side of Eq. (S40) is given by

$$\lim_{h \rightarrow 0} \frac{h^{n-1}}{h^{n-1}} z_p^{x-x_c-n+1} \binom{x-x_c}{n-1} + \mathcal{O}(h) = \frac{e^{-(x-x_c-n+1)/\xi_p}}{(n-1)!} \prod_{\mu=1}^{n-1} (x-x_c-\mu+1). \quad (\text{S42})$$

The PLE interaction manifests itself in the power-law factor $\prod_{\mu=1}^{n-1} (x-x_c-\mu+1)$, which originates mathematically from the existence of n -order zero of $h(z)$, and physically from the superposition of n exponential decay components with the same decay length ξ_p . Note that, similar fashion can also apply to the interaction for $x < x_c$, e.g., one just needs to consider the higher-order zeros of $h(z)$ outside the unit circle, which leads to the PLE interaction with left chirality.

Now generalizing the results to a generic lattice, whose distribution of zeros of the characteristic polynomial $h(z)$ is arbitrary. The d-d interaction mediated by such lattice can be rewritten as

$$\langle x | \varphi_E \rangle = \begin{cases} \langle x \geq x_c | \varphi_E \rangle = \frac{1}{\mathcal{N}} \sum_{\mu=1}^{n_\mu-1} \sum_{\alpha=0}^{n_\mu-1} r_{\mu\alpha} (x-x_c)^\alpha e^{-(x-x_c)/\xi_\mu} \\ \langle x < x_c | \varphi_E \rangle = \frac{1}{\mathcal{N}} \sum_{\nu=1}^{n_\nu-1} \sum_{\beta=0}^{n_\nu-1} l_{\nu\beta} (x-x_c)^\beta e^{-(x-x_c)/\xi_\nu} \end{cases}. \quad (\text{S43})$$

Here the indices μ and ν cover respectively all the distinctive zeros of $h(z)$ inside and outside the unit circle, associating with the orders n_μ and n_ν . Thus $\sum_\mu n_\mu = P + W$, $\sum_\nu n_\nu = Q - W$, and $\xi_{\mu,\nu} = -1/\ln(z_{\mu,\nu})$ denote the decay length. The constants $r_{\mu\alpha}$ and $l_{\nu\beta}$ can be straightforwardly evaluated as

$$r_{\mu\alpha} = \frac{\Theta(\text{Re } \xi_\mu)}{(n_\mu-1)!} \sum_{i=\alpha-1}^{n_\mu-1} \binom{n_\mu-1}{i} S_1(i, \alpha-1) e^{-i/\xi_\mu} f_\mu^{(n_\mu-i-1)}(z_\mu), \quad (\text{S44a})$$

$$l_{\nu\beta} = \frac{-\Theta(-\text{Re } \xi_\nu)}{(n_\nu-1)!} \sum_{j=\beta-1}^{n_\nu-1} \binom{n_\nu-1}{j} S_1(j, \beta-1) e^{j/\xi_\nu} f_\nu^{(n_\nu-j-1)}(z_\nu), \quad (\text{S44b})$$

where $f_\mu(z) = \prod_{\nu \neq \mu} (z - z_\nu)^{-n_\nu}$, $S_1(\bullet, \bullet)$ is the Stirling numbers of the first kind, and $\Theta(x)$ is the Heaviside function. With the solution of edge state, we can evaluate the d-d interaction together with Eq. (S32) as $J(x_{1,A}, x_{2,A}) = 0$ and

$$J(x_{1,A}, x_{2,B}) \approx \lambda \sqrt{\eta^{-1}} \sqrt{1 - \eta^{-1}} \langle x | \varphi_E \rangle, \quad (\text{S45})$$

which recovers Eq. (2) in main text up to the constant factor $\sqrt{\eta^{-1}} \sqrt{1 - \eta^{-1}}$. Applying Eqs. (S43-S44) to the example we considered in main text also recovers Eq. (4).

According to Eq. (S42), the existence of n -order zero of $h(z)$, namely the superposition of n exponential components with the same decay length will lead to the PLE interaction with maximum power-law exponent $n - 1$. This gives the upper bound for the power-law exponents of PLE interaction in Eq. (S43)

$$\max_{\text{Re } \xi_\mu > 0} \{n_\mu\} \leq P + W, \quad \max_{\text{Re } \xi_\nu < 0} \{n_\nu\} \leq Q - W, \quad (\text{S46})$$

which recover Eq. (3) in main text.

B. Edge state without chirality

The bath Hamiltonian in the previous subsection possess chiral symmetry respected with σ_z , which results in the asymmetric distribution of the zero-energy edge state around the QE. Now, let's consider the other case of bath Hamiltonian $H_b(k) = d_y(k)\sigma_y + d_z(k)\sigma_z$ possessing chiral symmetry respected with σ_x , i.e., $\sigma_x^{-1} H_b(k) \sigma_x = -H_b(k)$. Since the chiral symmetry around $E = 0$, the QE still acts equivalently as a hard-core potential $V = \epsilon |x_{1,A}\rangle \langle x_{1,A}|$ with $\epsilon = \lambda^2 / (E_q - \omega_0) = \infty$, which guarantees the zero energy solution $[H_b + V] |\varphi_E\rangle = 0 |\varphi_E\rangle$. As a consequence of symmetry σ_x , the zero energy has equal components on each sublattice. This can be quickly proven as $(|\varphi_E\rangle = \sum_n (a_n \ b_n)^T \otimes |n\rangle)$

$$H \sum_n \begin{pmatrix} a_n \\ b_n \end{pmatrix} |n\rangle = 0 = -H \sum_n \begin{pmatrix} b_n \\ a_n \end{pmatrix} |n\rangle, \quad (\text{S47})$$

which results in $|a_n| = |b_n|$.

To solve the eigenequation, we first perform an spin-rotation transformation $\mathcal{R}_{\mathbf{e}_y}(-\pi/2) = \oplus_{x=-L/2}^{L/2} R_{\mathbf{e}_y}(-\pi/2)$ with $R_{\mathbf{n}}(\theta) = \exp(i\theta \boldsymbol{\sigma} \cdot \mathbf{n}/2)$ that only acts on the internal degrees of bath, then we have

$$[H_b^{\text{rot}} + V^{\text{rot}}] |\varphi_E^{\text{rot}}\rangle = 0 |\varphi_E^{\text{rot}}\rangle, \quad (\text{S48})$$

where the rotated potential and eigenstate

$$V^{\text{rot}} = \frac{\epsilon}{2} (|x_{1,A}\rangle \langle x_{1,B}|) \begin{pmatrix} 1 & 1 \\ 1 & 1 \end{pmatrix} \begin{pmatrix} \langle x_{1,A} | \\ \langle x_{1,B} | \end{pmatrix}, \quad |\varphi_E^{\text{rot}}\rangle = \mathcal{R}_{\mathbf{e}_y}^\dagger \left(-\frac{\pi}{2}\right) |\varphi_E\rangle. \quad (\text{S49})$$

One can easily verify that the bulk Hamiltonian $H_b^{\text{rot}}(k)$ has the form

$$H_b^{\text{rot}}(k) = R_{\mathbf{e}_y}(-\pi/2) H_b(k) R_{\mathbf{e}_y}^\dagger(-\pi/2) = -d_z(k)\sigma_x + d_y(k)\sigma_y = \begin{pmatrix} 0 & h_{\text{rot}}(k) \\ h_{\text{rot}}^*(k) & 0 \end{pmatrix}, \quad (\text{S50})$$

which restores the chiral symmetry $\sigma_z H_b^{\text{rot}}(k) \sigma_z^{-1} = -H_b^{\text{rot}}(k)$. Two important results about the edge state $|\varphi_E^{\text{rot}}\rangle$ can be already extracted. i) Our analysis for the spatial profile in last subsection also holds for $|\varphi_E^{\text{rot}}\rangle$, since the rotated Hamiltonian H_b^{rot} has chiral symmetry respected with σ_z . ii) $|\varphi_E^{\text{rot}}\rangle$ (namely $|\varphi_E\rangle$) has symmetric distribution around the atom since the parity symmetry of system is restored. To be more quantitative, Eq. (S35) is now rewritten as

$$h_{\text{rot}}(z) \Phi_B^{\text{rot}}(z) + \frac{\epsilon}{2} (\langle x_{1,A} | \varphi_E^{\text{rot}} \rangle z^{-x_{1,A}} + \langle x_{1,B} | \varphi_E^{\text{rot}} \rangle z^{-x_{1,B}}) = 0, \quad (\text{S51a})$$

$$h_{\text{rot}}^*(z^{-1}) \Phi_A^{\text{rot}}(z) + \frac{\epsilon}{2} (\langle x_{1,A} | \varphi_E^{\text{rot}} \rangle z^{-x_{1,A}} + \langle x_{1,B} | \varphi_E^{\text{rot}} \rangle z^{-x_{1,B}}) = 0. \quad (\text{S51b})$$

Thus, the rotated edge state $|\varphi_E^{\text{rot}}\rangle$ on sublattice B has the same form as the expression we derived in the previous subsection. Moreover, $h_{\text{rot}}^*(z^{-1})$ possesses inverse plus conjugate zeros and poles compared to $h_{\text{rot}}(z)$, i.e., a pole at z_i of $h_{\text{rot}}(z)$ corresponds to a pole at $1/z_i^*$ of $h_{\text{rot}}^*(z^{-1})$ and vice versa. The distribution for zeros and poles between

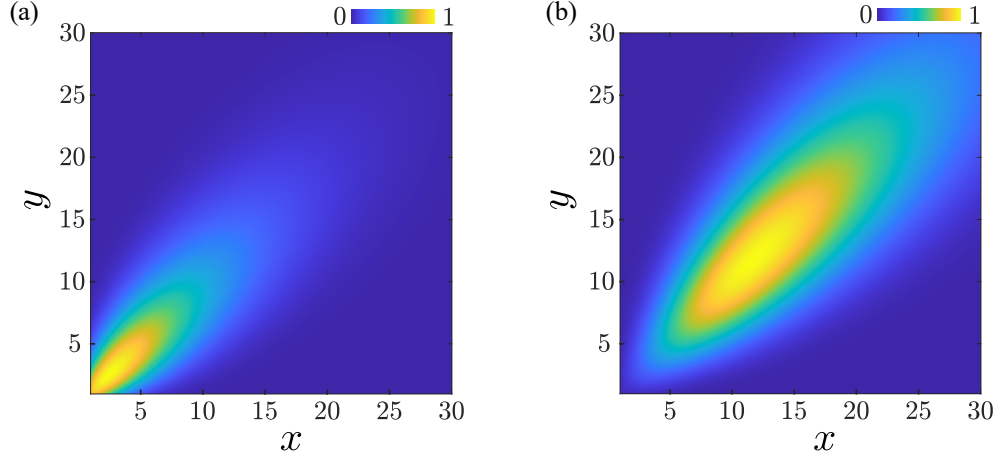


FIG. S3: Interaction obtained from Eq. (S58) and Eq. (S59) are shown in (a) and (b), respectively. The interaction strengths were rescaled to its maximum values. The factorial function has been replaced by the gamma function to obtain the continuous spatial profile.

$h_{\text{rot}}(z)$ and $h_{\text{rot}}^*(z^{-1})$ eventually leads to the inverse plus conjugate spatial profile between $\langle x_{2,A} | \varphi_E^{\text{rot}} \rangle$ and $\langle x_{2,B} | \varphi_E^{\text{rot}} \rangle$, i.e.,

$$\langle x_A | \varphi_E^{\text{rot}} \rangle = \langle \varphi_E^{\text{rot}} | x_B \rangle, \quad x_A = -x_B, \quad (\text{S52})$$

where the relative distance $x_A = x_{2,A} - x_{1,A}$ and $x_B = x_{2,B} - x_{1,B}$. The final step to obtain the edge state is a inverse rotation to $\langle x_{A/B} | \varphi_E^{\text{rot}} \rangle$

$$|\varphi_E\rangle = \oplus_x R_y\left(-\frac{\pi}{2}\right) \begin{pmatrix} \langle x_A | \varphi_E^{\text{rot}} \rangle |x_A\rangle \\ \langle x_B | \varphi_E^{\text{rot}} \rangle |x_B\rangle \end{pmatrix}, \quad (\text{S53})$$

which gives the edge state without chirality

$$|\langle x_A | \varphi_E \rangle| = \frac{1}{\sqrt{2}} |\langle \varphi_E^{\text{rot}} | -x_A \rangle - \langle x_A | \varphi_E^{\text{rot}} \rangle| = |\langle -x_A | \varphi_E \rangle|, \quad |\langle x_B | \varphi_E \rangle| = \frac{1}{\sqrt{2}} |\langle \varphi_E^{\text{rot}} | -x_B \rangle + \langle x_B | \varphi_E^{\text{rot}} \rangle| = |\langle -x_B | \varphi_E \rangle|. \quad (\text{S54})$$

The obtained edge states are just the linear combination of the edge states we obtained in previous subsection, thus the corresponding power-law exponent can only either be invariant or decreasing. The upper bound for right-side component $\langle x_{A/B} \geq 0 | \varphi_E \rangle$ is determined by $\max\{P_{\text{rot}} + W, Q_{\text{rot}} - W\}$ where P_{rot} and Q_{rot} are the hopping parameters associated with H_b^{rot} , and W is the winding number corresponding to H_b^{rot} . The same conclusion holds for left-side component due to the parity symmetry of edge states.

III. POWER-LAW ENHANCED INTERACTION IN HIGHER DIMENSIONAL LATTICE

In this subsection, we demonstrate the implement of power-law enhanced interaction in 2D square lattice. Our conclusion can also be applied to higher-dimensional lattice bath. We do not refer to “PLE” interaction for reasons will be given latter. For theoretical simplification, the 2D square lattice under consideration respect chiral symmetry σ_z , i.e., $\sigma_z H(k_x, k_y) \sigma_z = -H(k_x, k_y)$, such that the VDS mechanism is valid and the equations for state components on different sublattice are decoupled. The full properties of the lattice are encoded in $h(k_x, k_y)$. We assume the QE couples to lattice in sublattice A of position $(0, 0)$. It is known that a gapless lattice in higher dimension can also produce coherent d-d interaction, due to the vanishing density of states [6, 7]. However, we here consider the gapped lattice, which means that $h(z_1, z_2) \neq 0$ for any point z_1, z_2 on the 2D circle surface. Taking similar fashion in section II, we have

$$J(\mathbf{r}_B) \propto \langle \mathbf{r}_B | \varphi_E \rangle \propto \frac{1}{(2\pi i)^2} \oint_{|z_1|=1} \oint_{|z_2|=1} \Phi_B(z_1, z_2) z_1^{x-1} z_2^{y-1} dz_1 dz_2 \quad (\text{S55})$$

and $\Phi_A(z_1, z_2) = 0$, where $\mathbf{r}_{A/B} = (x, y)$ denotes the position vector in sublattice A/B . The integral contours can be chosen to be the individual unit circle since we consider a gapped lattice. One can easily show that the generic form of $\Phi_B(z_1, z_2)$ is

$$\Phi_B(z_1, z_2) = \frac{1}{h(z_1, z_2)} = \frac{1}{\sum_{ij} t_{ij} z_1^i z_2^j}, \quad (\text{S56})$$

where $h(z_1, z_2) \equiv h(k_x \rightarrow -i \ln z_1, k_y \rightarrow -i \ln z_2)$. The expression for $h(z_1, z_2)$ can be obtained as i) a p_x -site (q_x -site) hopping from sublattice A to B towards left (right) direction contributes a $z_1^{-p_x}$ ($z_1^{q_x}$); ii) a p_y -site (q_y -site) hopping from sublattice A to B towards up (down) direction contributes a $z_2^{-p_y}$ ($z_2^{q_y}$). Thereby, the coefficient t_{ij} denotes the hopping strength of lattice.

Unlike the 1D lattice we consider in main text, in which the form of dressed bound state can be explicitly solved for arbitrary configuration of lattice owing to the *Fundamental Theorem of Algebra*, as long as the hopping range is finite. In 2D geometry, this theorem fails for a two variables characteristic polynomial $h(z_1, z_2)$, thus Eq. (S55) can barely be evaluated even for simple lattice configuration. Nonetheless, the analog of PLE interaction in 1D lattice, namely the power-law enhanced interaction, can be obtained as

$$J'(\mathbf{r}_B) = x^\alpha y^\beta J(\mathbf{r}_B) \propto \frac{1}{(2\pi i)^2} \oint_{|z_1|=1} \oint_{|z_2|=1} z_1^{x-1} z_2^{y-1} \mathcal{D}^\alpha(z_1) \mathcal{D}^\beta(z_2) \Phi_B(z_1, z_2) dz_1 dz_2, \quad (\text{S57})$$

where we introduce the operator $\mathcal{D}(z) = z\partial/\partial z$. In other word, the d-d interaction mediated by the new lattice with the characteristic function $h'(z_1, z_2) = (\mathcal{D}^\alpha(z_1) \mathcal{D}^\beta(z_2) h^{-1}(z_1, z_2))^{-1}$ has power-law enhancement $x^\alpha y^\beta$ compared with the d-d interaction in the original lattice with $h(z_1, z_2)$. Clearly, one can regard the PLE interaction in 1D as a special case of power-law enhanced interaction, where the original exponential decay interaction $J(x)$ are enhanced by the power-law factor, thus leads to $J'(x) \propto x^\alpha \exp(-x/\xi)$. Despite the power-law enhanced behavior similar to PLE interaction in 1D, there are no corresponding upper bounds for power-law exponents α, β in 2D lattice. This is again, due to the failure of *Fundamental Theorem of Algebra* in 2D geometry.

We present a solvable model to demonstrate the power-law enhanced interaction in 2D. To this end, we consider an original lattice with $h(k_x, k_y) = t_{0,0} + t_{-1,0} \exp(-ik_x) + t_{0,-1} \exp(-ik_y)$. When hopping strengths satisfy $|t_{-1,0}| + |t_{0,-1}| < |t_{0,0}|$, the resulted d-d interaction can be obtained as

$$J(\mathbf{r}_B) \propto e^{-x/\xi_x} e^{-y/\xi_y} F(x, y), \quad x, y \geq 0, \quad (\text{S58})$$

where the interaction length $\xi_x = -\ln(t_{-1,0}/t_{0,0})$ and $\xi_y = -\ln(t_{0,-1}/t_{0,0})$, $F(x, y) = (x+y)!/x!y!$. The power-law enhanced interaction with power-law exponent 1 in both x and y direction

$$J'(\mathbf{r}_B) \propto xye^{-x/\xi_x} e^{-y/\xi_y} F(x, y), \quad x, y \geq 0 \quad (\text{S59})$$

can be mediated by the lattice with bulk Hamiltonian $h'(k_x, k_y) = (t_{0,0} + t_{-1,0} \exp(-ik_x) + t_{0,-1} \exp(-ik_y))^3 \exp(ik_x + ik_y)$. As shown in Fig. S3, the spatial profiles of $J'(\mathbf{r}_B)$ exhibits non-monotonic behavior in this case, just as the PLE interaction in 1D lattice.

IV. TOPOLOGICAL PROTECTION OF PLE INTERACTION

In this section, we explore whether the PLE interaction inherits the topological protection feature from edge state. To do that, we study the robustness of the topological dressed bound state against disorder since this dressed bound state possesses the same spatial profile with PLE interaction. We consider two types of disorder depending on whether they preserve the chiral symmetry or not and present the results in Fig. S4. As expected, the topological bound states exhibit robustness against symmetry-preserving disorder. Besides, the shape of dressed bound states is more sensitive to symmetry-breaking disorder in comparison with symmetry-preserving disorder. Nonetheless, the dressed bound states retain qualitatively the non-monotonic behavior for both symmetry-preserving and symmetry-breaking disorder.

Specifically, for bath Hamiltonian given in Fig. 1(b) of main text, the chiral symmetry is σ_z , the obtained dressed bound states exhibit unidirectional spatial profile and has support in one of the sublattices in the clean limit. The

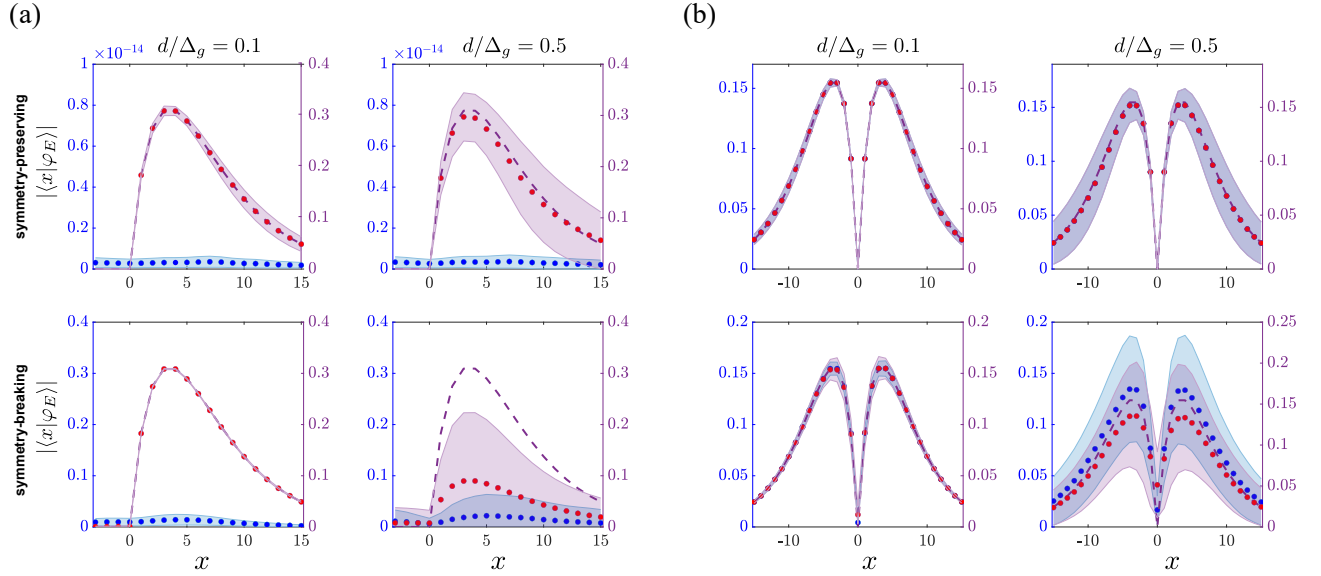


FIG. S4: (a-b) PLE dressed bound states for Hamiltonian Eq. (S60) and Eq. (S61), respectively. The red (blue) dots denote components on sublattice B (A) under 10^3 disorder realizations, while shadow areas span their corresponding standard deviation. Dashed lines are PLE state in the clean limit, and we only plot clean PLE state on sublattice B in (a) since the zero components on sublattice A. In all plots, parameters are chosen to be $\lambda/\Delta_g = 2.3$, and $\Delta_g = 0.13$.

x	-3	-2	-1	0	1	2	3
$ \langle x_A \varphi_E \rangle $	0.152171	0.135736	0.090647	0	0.090547	0.135833	0.152052
$ \langle x_B \varphi_E \rangle $	0.152171	0.135736	0.090647	0	0.090547	0.135833	0.152052

TABLE S1: PLE dressed bound state corresponds to data shown in Fig. S4(b) with symmetry-preserving disorder and $d/\Delta_g = 0.5$.

disorder is implemented as $H_b \rightarrow$

$$\begin{cases} H_b + \sum_j \varepsilon_{1,j} a_{j,B}^\dagger a_{j+1,A} + \sum_j \varepsilon_{2,j} a_{j,A}^\dagger a_{j,B} + \sum_j \varepsilon_{3,j} a_{j,A}^\dagger a_{j+1,B} + h.c., & \text{symmetry preserving,} \\ H_b + (\sum_j \varepsilon_{1,j} a_{j,A}^\dagger a_{j,A} + \sum_j \varepsilon_{2,j} a_{j,B}^\dagger a_{j,B})/2 + \sum_j \varepsilon_{3,j} a_{j,A}^\dagger a_{j+1,A} + \sum_j \varepsilon_{4,j} a_{j,B}^\dagger a_{j+1,B} + h.c., & \text{symmetry breaking} \end{cases} \quad (\text{S60})$$

The coefficients $\varepsilon_{1-4,j}$ are i.i.d random variables, drawing from Gaussian distribution $\mathcal{N}(0, d)$. For symmetry-preserving disorder, the topological properties of dressed bound state, i.e the unidirectionality and the zero component on sublattice A [see the top of Fig. S4(a)], retain as expected from the mechanism of vacancy-like dressed bound state. For symmetry-breaking disorder, the resulted dressed bound state lost its unidirectionality and has non-zero component on each sublattices [see the bottom of Fig. S4(a)]. Moreover, the shape of bound state retains its non-monotonic behavior both for symmetry-preserving and symmetry-breaking disorder. The shape is more sensitive to symmetry-breaking disorder comparing with symmetry-preserving disorder, i.e., it has larger deviation from its clean counterpart for symmetry-breaking disorder.

For bath Hamiltonian given in Fig. 1(c) of main text, the chiral symmetry is σ_x . As a consequence of chiral symmetry σ_x , the obtained dressed bound state has equal weight on each sublattice of lattice. The disorder is implemented as $H_b \rightarrow$

$$\begin{cases} H_b + \sum_j \varepsilon_{1,j} a_{j,A}^\dagger a_{j,A} - \sum_j \varepsilon_{1,j} a_{j,B}^\dagger a_{j,B}, & \text{symmetry preserving,} \\ H_b + (\sum_j \varepsilon_{1,j} a_{j,A}^\dagger a_{j,A} + \sum_j \varepsilon_{2,j} a_{j,B}^\dagger a_{j,B})/2 + \sum_j \varepsilon_{3,j} a_{j,A}^\dagger a_{j,B} + h.c., & \text{symmetry breaking} \end{cases} \quad (\text{S61})$$

The coefficients $\varepsilon_{1-3,j}$ are i.i.d random variables, drawing from Gaussian distribution $\mathcal{N}(0, d)$. For symmetry-preserving disorder, the dressed bound states have equal components on sublattice A and B at each unit cell [see

Table. S1 and the top of Fig. S4(b)]. When the introduced disorder breaks the chiral symmetry of bath Hamiltonian, the dressed bound states lost the property [see the bottom of Fig. S4(b)]. Similar to the former case, the shape of bound state retains its non-monotonic behavior both for symmetry-preserving and symmetry-breaking disorder.

V. PLE INTERACTION WITH THE HIGHER POWER-LAW EXPONENT

Our analytical derivation in the main text claims that the largest power-law exponent of interaction is upper bounded by $P + W - 1$ (here we consider the completely chiral case which implies $Q - W = 0$ for simplicity). Therefore, one firstly need to increase $P + W$ to obtain a PLE interaction with a higher power-law exponent. For example, one can add the long (but finite)-range hopping to increase P . After that, the bath needs to be fine-tuning to generate the high-order zeros of $h(z)$ in order to obtain a higher power-law exponent for a given bound.

Here we illustrate the PLE interaction with maximal power-law exponent of 3. This requires the next-next-nearest neighbor hopping between cells of bath [see Fig. S5]. As observed in Fig. S5, the PLE decay edge state is obtained by tuning bath parameters to $h(k) = (e^{ik} - 3/5)^4 / e^{3ik}$, as shown in Fig. S5(a).

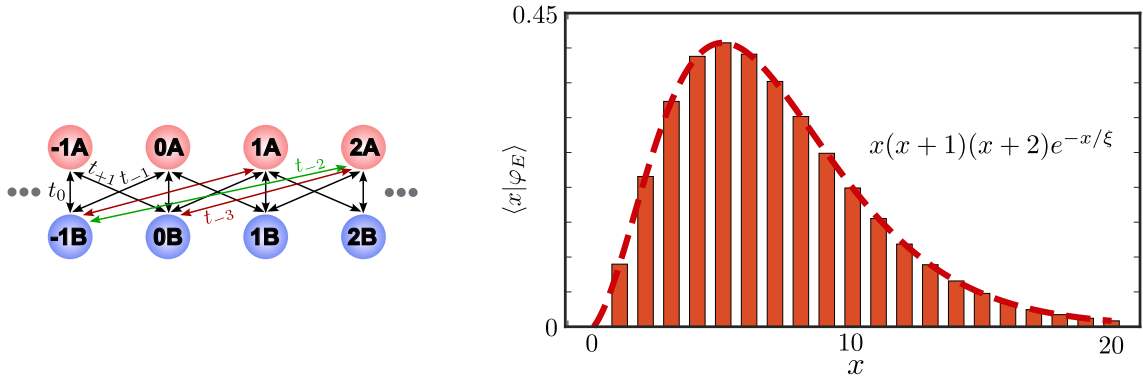


FIG. S5: Right plot shows the chiral PLE edge state corresponded to bath Hamiltonian with $h(k) = (e^{ik} - 3/5)^4 / e^{3ik}$, which corresponds to the chiral PLE d-d interaction with $\xi = -1/\ln(0.6)$. The histogram and dashed line is drawn from the numerical and analytical solution, respectively. Left plot shows the configuration with $t_{-3}/t_0 = -27/500$, $t_{-2}/t_0 = -9/25$, $t_{-1}/t_0 = -9/10$, $t_{+1}/t_0 = -5/12$.

VI. FURTHER DISCUSSION ABOUT THE MANY-BODY PHASES

In this section, we discuss the many-body phases of XXZ model $H_{XXZ} = \sum_{m>n} J(m-n)(S_m^+ S_n^- / 2 + S_m^- S_n^+ / 2 + J_z S_m^z S_n^z)$ for PLE interaction $J(x) = x \exp(-x/\xi)$, exponential decay interaction $J(x) = \exp(-x/\xi)$ and power-law decay interaction $J(x) = x^{-\xi}$. The phase diagrams are shown in Figs. S6(a-c), and the correlation functions in each phase are shown in Figs. S6(d-e). The phase diagrams clearly indicate that the AFM(T) and QLRO(T) phases only occur in PLE interacting system, which supports our statement in main text. In subsections A and B, we present the detailed methods for obtaining these phases diagrams and the phase boundaries.

A. FM phase and its boundary

We analytically calculate the FM phase boundary via a spin-wave analysis. For $J_z \ll 0$, one should expect all spins are polarized along the $+z$ direction. Thus, we treat $|\uparrow\uparrow\cdots\uparrow\rangle$ as the vacuum state with no excitations and apply the Holstein-Primakoff transformation $S_j^z = 1/2 - a_j^\dagger a_j$, $S_j^+ = a_j$, $S_j^- = a_j^\dagger$, where $[a_i, a_j^\dagger] = \delta_{ij}$.

In the weak excitation limit, $\langle a_j^\dagger a_j \rangle \ll 1$, the XXZ Hamiltonian under PLE interaction becomes

$$H_{XXZ} \approx \frac{1}{2} \sum_{m>n} (m-n) e^{-(m-n)/\xi} (a_m^\dagger a_n + a_n^\dagger a_m - J_z (a_m^\dagger a_m + a_n^\dagger a_n)). \quad (\text{S62})$$

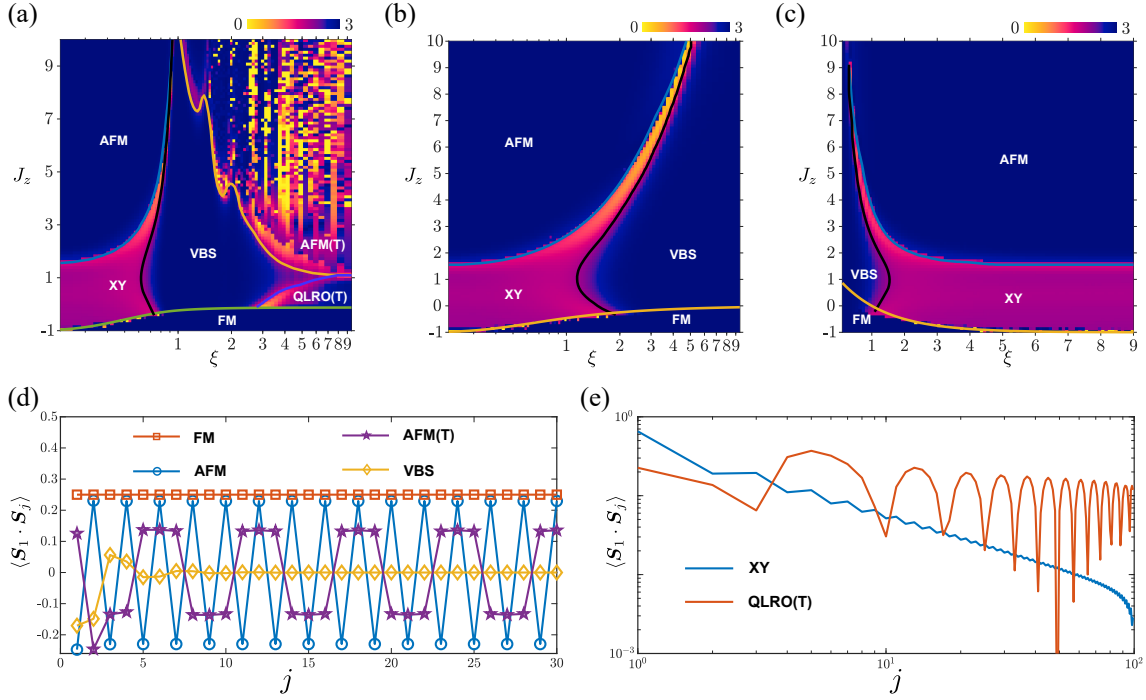


FIG. S6: (a-c) Effective central charge for PLE (a), exponential decay (b) and power-law decay (c) interacting systems. In all plots, we have set the maximum value of c_{eff} to 3. The white circles correspond the position where the spin correlation functions in (d-e) are drawn from. (d) Spin correlation deep in gapped phases. (e) Spin correlation deep in gapless phases.

In the thermodynamic limit $N \rightarrow \infty$, one can diagonalize this Hamiltonian to $H_{\text{PLE}} = \int dk \omega_k c_k^\dagger c_k$ for $k \in (-\pi, \pi]$ with the following dispersion relation

$$\omega_k = \frac{-J_z e^{-1/\xi}}{(-1 + e^{-1/\xi})^2} + \frac{e^{-1/\xi}((1 + e^{-2/\xi}) \cos(k) - 2e^{-1/\xi})}{(1 + e^{-2/\xi} - 2e^{-1/\xi} \cos(k))^2}. \quad (\text{S63})$$

The $\omega_{\min} \equiv \min \omega(k) = 0$ condition sets the phase boundary. For dispersion Eq. (S63), $\omega_{\min} = \omega(k = \pi)$ for $\xi \leq -1/\log(2 - \sqrt{3})$ and $\omega_{\min} = \omega(k = \pm k_0)$ for $\xi > -1/\log(2 - \sqrt{3})$ where

$$k_0 = \arctan\left(\frac{\sqrt{-(e^{-4/\xi} - 14e^{-2/\xi} + 1)(e^{-2/\xi} - 1)^2}}{-e^{-4/\xi} + 6e^{-2/\xi} - 1}\right). \quad (\text{S64})$$

Then, the boundary can be obtained by solving $\omega_{\min} = 0$, which gives

$$J_z = \frac{(e^{-1/\xi} - 1)^2((1 + e^{-2/\xi}) \cos(\text{Re}(k_0)) - 2e^{-1/\xi})}{(1 + e^{-2/\xi} - 2e^{-1/\xi} \cos(\text{Re}(k_0)))^2}. \quad (\text{S65})$$

For exponential decay and power-law decay interacting systems, similar fashion applied and we can obtain the corresponding dispersion relations as

$$\omega_k = \frac{-J_z e^{-1/\xi}}{-1 + e^{-1/\xi}} - \frac{e^{-1/\xi}(1 + e^{2ik} - 2e^{ik-1/\xi})}{2(e^{ik} - e^{-1/\xi})(-1 + e^{ik-1/\xi})} \quad (\text{S66})$$

and

$$\omega_k = -J_z \sum_{r=1}^{\infty} \frac{1}{r^\xi} + \sum_{r=1}^{\infty} \frac{\cos(kr)}{r^\xi}, \quad (\text{S67})$$

respectively. The minima of ω_k for both exponential decay and power-law decay interactions appear at $k = \pi$. Therefore, the boundary can be solved as

$$J_z = \frac{e^{-1/\xi} - 1}{e^{-1/\xi} + 1} \quad (\text{S68})$$

and

$$J_z = \text{Li}_\xi(-1)/\zeta(\xi), \quad \xi > 1, \quad (\text{S69})$$

respectively. Here $\text{Li}_s(z)$ the polylogarithm function and $\zeta(z)$ the Riemann zeta function. Note that, the obtained boundary for power-law decay interaction is $J_z = 0$ for $\xi \leq 1$, since the FM state's energy is super extensive [8].

B. Other phase boundaries

We extract the phase boundaries by numerically calculating the effective central charge c_{eff} of ground state [9]. The XY phase is described by conformal field theory with the actual central charge $c = c_{\text{eff}} = 1$. In other phases with no conformal symmetry, c_{eff} does not have the meaning of the central charge and is used only as a diagnostic here to numerically find phase boundaries.

The XY-to-AFM and XY-to-VBS phase boundaries are numerically obtained by finding the place where c_{eff} starts to decrease 0.04 below $c_{\text{eff}} = 1$. The VBS-to-AFM(T) and VBS-to-QLRO(T) phase boundaries are numerically obtained by finding the place where c_{eff} starts to increase from $c_{\text{eff}} = 1$.

VII. DISCUSSION OF EXPERIMENTAL IMPLEMENTATION OF PLE INTERACTION

In this section, we discuss the experimental implication of the PLE interaction. Fig. S7(a) shows the full circuit model used in the simulations of Eq. (1).

The parameters $C_0, C_v, C_w, M_v, M_w, L_0 = 253 \text{ fF}, 42 \text{ fF}, 8 \text{ fF}, -11 \text{ pH}, -24 \text{ pH}, 1.9 \text{ nH}$ are adopted from the experimental work in [10]. The longer-range hopping beyond nearest-neighbor could be implemented by introducing the capacitor $C_p = 39 \text{ fF}$. Given the values of these circuit elements, the corresponding parameters of the topological waveguide QED system displayed in Fig. S7 can be obtained as $\omega_0/2\pi \approx 10 \text{ GHz}$, $t_0/2\pi \approx t_{+1}/2\pi \approx 400 \text{ MHz}$ and $t_{-1}/2\pi \approx 113 \text{ MHz}$. Since the d-d interaction can be recovered by the single QE dressed bound state according to $J(x) \propto \lambda \langle x | \varphi_E \rangle$, we assume that only one QE is resonantly coupled to bath in sublattice A at the middle of chain, with chain size $L = 20$ and coupling strength $\lambda/2\pi = 90 \text{ MHz}$. The spectrum of system contains 41 eigenvalues in single-excitation regime. Except the bulk state energies, two in-gap energies $\approx -1.37, 0 \text{ MHz}$ corresponding to the edge states of bath appear [see the red circles in Fig. S8(a)]. Moreover, due to the finite size bath, the dressed bound state energies $\approx 1.37 \text{ MHz}$ [see the red square in Fig. S8(a)] is slightly deviated from the analytical prediction $E = 0$. In spite of the small size bath, the obtained PLE interaction [see Fig. S8(b)] by numerically calculation consist with the analytical prediction up to a constant correction. This correction mainly originates from the non-zero occupation of dressed bound state in sublattice A, due to the open boundary condition in small bath size. Therefore, our results show that the PLE interaction can be implemented in the current experimental platform in small bath size.

Since the most important element to implement PLE interaction is the longer-range hopping terms beyond nearest-neighbor of bath. We introduce another proposal to implement long-rang hopping term based on [11]. The basic idea is that the LC resonators representing lattice sites are coupled in groups to auxiliary resonators according to

$$H_{\text{tot}} = \sum_{\mu=\text{I,II},\dots} \sum_{\langle \alpha \rangle_\mu} g(t) c_\alpha^\dagger b_\mu e^{i(\omega_\alpha - \omega_{\text{aux}})} + h.c. \quad (\text{S70})$$

with time-dependent coupling $g(t) \propto \sum_i A_i \cos(\Omega_i t)$. Here the notation $\langle \alpha \rangle$ denotes the summation over the sites α connected by auxiliary cavity μ . Then, under weak coupling approximation $|\omega_\alpha - \omega_{\text{aux}}| \gg |\omega_\alpha - \omega_\beta| \gg |g(t)|$, the long-range hopping terms of lattice bath can be obtained by adiabatically eliminating the auxiliary cavity as

$$H_{\text{eff}} \approx \frac{1}{2} \sum_{i,j} \frac{A_i A_j}{4} \left(e^{i(\Omega_i + \Omega_j)t} + e^{i(\Omega_i - \Omega_j)t} + c.c. \right) \sum_{\mu, \langle \alpha, \beta \rangle_\mu} \left(\frac{1}{\omega_{\text{aux}} - \omega_\alpha} + \frac{1}{\omega_{\text{aux}} - \omega_\beta} \right) c_\alpha^\dagger c_\beta e^{-i(\omega_\alpha - \omega_\beta)t} + h.c.. \quad (\text{S71})$$

Then, one can obtain the desired long-range hopping by taking the frequencies satisfying the resonant conditions $\Omega_i \pm \Omega_j = (\pm)(\omega_\alpha - \omega_\beta)$, while the undesired hopping terms with the off-resonant frequencies will be greatly suppressed due to the weak coupling approximation.

For the bath configuration in Fig. 1(b) of main text, we couple six lattice sites in groups to the auxiliary resonators, and with the energy distribution shown in Fig. S7(b). One can chose the frequencies according to (consider the first auxiliary cavity and coupled sites for simply)

$$\Omega_{1,2}^+ = \Delta_{1,4}, \quad \Omega_{2,3}^+ = \Delta_{3,6}, \quad \Omega_{4,5}^+ = \Delta_{1,2}, \quad \Omega_{4,6}^+ = \Delta_{2,3}, \quad \Omega_{5,6}^+ = \Delta_{4,5}, \quad \Omega_{1,3}^+ \neq \Delta_{2,5}, \quad (\text{S72})$$

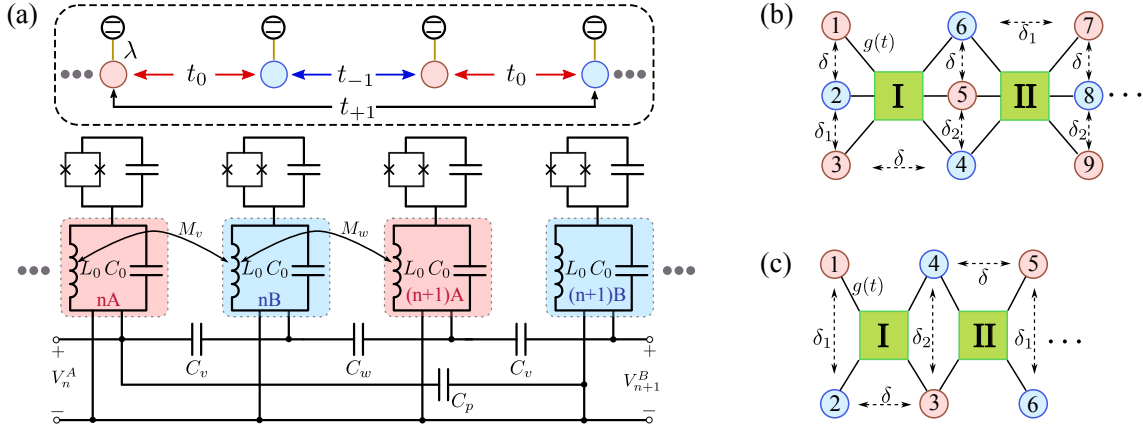


FIG. S7: (a) Full circuit model used in the simulations of Eq.(1) with bath configuration shown in Fig.1(b) of main text, we assume that each site couples an emitter, the parameters are further discussed in the text. (b-c) Possible circuit QED architectures to implement the bath Hamiltonian in Fig.1(b) (see (b)) and Fig.1(c) (see (c)) of main text. A set of LC resonators with frequency ω_α is coupled in groups to auxiliary resonators (denoted by Roman numbers I, II ...) with frequency ω_{aux} and time-dependent coupling $g(t)$. The bare energies of lattice resonator ω_i have a distribution of energy difference denoted by $\delta, \delta_1, \delta_2$.

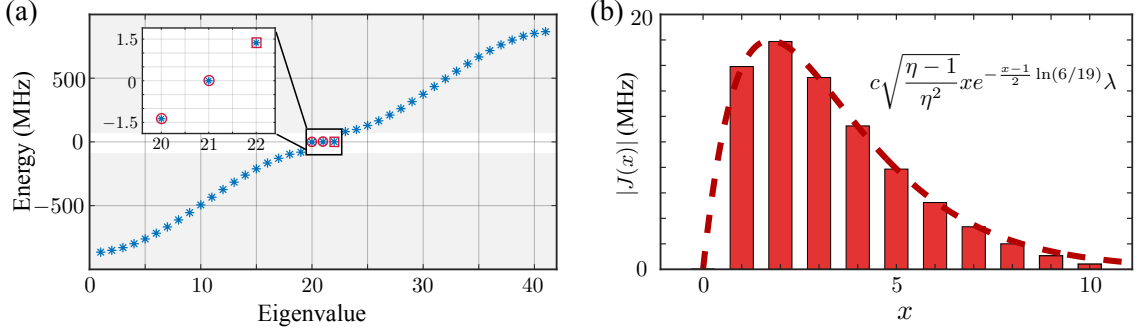


FIG. S8: (a) Schematic of QEs-waveguide model. Eigenspectrum of system in single-excitation regime, where we set $\omega_q = \omega_0 = 0$ for simplicity. The bath Hamiltonian under periodic condition is $H_b(k) = d_x(k)\sigma_x + d_y(k)\sigma_y$ with $h(k)/t_0 = (e^{ik} + \sqrt{6/19})^2 / e^{ik}$. The encircled stars represent edge state energies, and the dressed bound state energy is marked by the rectangle. (b) Spatial profile of d-d interaction. The histogram and dashed line correspond to the numerical solution and analytical prediction. Here $\eta \approx 1.26$, and the correction factor due to the open boundary condition is numerically fixed by $c \approx 0.8$.

where $\Omega_{i,j}^+ = \Omega_i + \Omega_j$ and $\Delta_{\alpha,\beta} = \omega_\alpha - \omega_\beta$. Under these conditions, only the hopping terms $c_m^\dagger c_n + h.c.$ for $(m,n) = \{(1,2), (3,4), (5,6)\}$ with the hopping strength t_0 , $(m,n) = \{(2,3), (4,5)\}$ with the hopping strength t_{-1} and $(m,n) = \{(1,4), (3,6)\}$ with the hopping strength t_{+1} are resonant, while others are off-resonant. Finally, the desired hopping terms with certain strengths $\{t_0; t_{-1}; t_{+1}\}$ can be implemented by taking $A_1 A_3 = t_{+1}$, $A_4 = A_5 = \sqrt{t_0}$, $A_6 = t_{-1}/t_0$.

For PLE interaction without chirality, i.e., the bath configuration in Fig.1(c) of main text, the set-up is different from the former case. Here we couple four lattice sites in groups to the auxiliary resonators, and with the energy distribution shown in Fig. S7(c). A possible resonant condition reads as

$$\Omega_{1,2}^+ = \Delta_{1,3}, \quad \Omega_{2,3}^+ = \Delta_{2,4}, \quad \Omega_4 = \Delta_{2,3}, \quad \Omega_{1,3}^+ \neq \Delta_{1,2} \quad (\text{S73})$$

associating with the amplitudes condition $A_1 A_2 = t'_0 = A_2 A_3$ and $A_4 = t'_1$ to obtain the desired hopping structure shown in main text.

* Electronic address: xinyoulu@hust.edu.cn

- [1] C. C. Tannoudji, G. Grynberg, and J. Dupont-Roe, *Atom-photon interactions* (New York, NY (United States); John Wiley and Sons Inc., 1992).
- [2] E. N. Economou, *Green's functions in quantum physics*, Vol. 7 (Springer Science & Business Media, 2006).
- [3] A. González-Tudela and J. I. Cirac, Non-Markovian Quantum Optics with Three-Dimensional State-Dependent Optical Lattices, *Quantum* **2**, 97 (2018).
- [4] T. Shi, Y.-H. Wu, A. González-Tudela, and J. I. Cirac, Bound states in boson impurity models, *Phys. Rev. X* **6**, 021027 (2016).
- [5] L. Leonforte, A. Carollo, and F. Ciccarello, Vacancy-like dressed states in topological waveguide qed, *Phys. Rev. Lett.* **126**, 063601 (2021).
- [6] A. González-Tudela and J. I. Cirac, Exotic quantum dynamics and purely long-range coherent interactions in dirac conelike baths, *Phys. Rev. A* **97**, 043831 (2018).
- [7] I. n. García-Elcano, A. González-Tudela, and J. Bravo-Abad, Tunable and robust long-range coherent interactions between quantum emitters mediated by weyl bound states, *Phys. Rev. Lett.* **125**, 163602 (2020).
- [8] Z.-X. Gong, M. F. Maghrebi, A. Hu, M. Foss-Feig, P. Richerme, C. Monroe, and A. V. Gorshkov, Kaleidoscope of quantum phases in a long-range interacting spin-1 chain, *Phys. Rev. B* **93**, 205115 (2016).
- [9] P. Calabrese and J. Cardy, Entanglement entropy and quantum field theory, *Journal of Statistical Mechanics: Theory and Experiment* **2004**, P06002 (2004).
- [10] E. Kim, X. Zhang, V. S. Ferreira, J. Banker, J. K. Iverson, A. Sipahigil, M. Bello, A. González-Tudela, M. Mirhosseini, and O. Painter, Quantum electrodynamics in a topological waveguide, *Phys. Rev. X* **11**, 011015 (2021).
- [11] C. Vega, M. Bello, D. Porras, and A. González-Tudela, Qubit-photon bound states in topological waveguides with long-range hoppings, *Phys. Rev. A* **104**, 053522 (2021).